RSC Advances

REVIEW

View Article Online
View Journal | View Issue

Check for updates

Cite this: *RSC Adv.*, 2023, **13**, 32381

Production, surface modification, physicochemical properties, biocompatibility, and bioimaging applications of nanodiamonds

Tirusew Tegafaw,[a] Shuwen Liu,[a] Mohammad Yaseen Ahmad,[a] Abdullah Khamis Ali Al Saidi,[a] Dejun Zhao,[a] Ying Liu,[a] Huan Yue,[a] Sung-Wook Nam,[b] Yongmin Chang*[b] and Gang Ho Lee *[a]

Nanodiamonds (ND) are chemically inert and stable owing to their sp^3 covalent bonding structure, but their surface sp^2 graphitic carbons can be easily homogenized with diverse functional groups *via* oxidation, reduction, hydrogenation, amination, and halogenation. Further surface conjugation of NDs with hydrophilic ligands can boost their colloidal stability and functionality. In addition, NDs are non-toxic as they are made of carbons. They exhibit stable fluorescence without photobleaching. They also possess paramagnetic and ferromagnetic properties, making them suitable for use as a new type of fluorescence imaging (FI) and magnetic resonance imaging (MRI) probe. In this review, we focused on recently developed ND production methods, surface homogenization and functionalization methods, biocompatibilities, and biomedical imaging applications as FI and MRI probes. Finally, we discussed future perspectives.

Received 8th October 2023
Accepted 26th October 2023

DOI: 10.1039/d3ra06837d

rsc.li/rsc-advances

Open Access Article. Published on 03 November 2023. Downloaded on 2/10/2026 5:30:09 AM.
This article is licensed under a Creative Commons Attribution-NonCommercial 3.0 Unported Licence.

Introduction

Over the past decades, many studies have demonstrated the potential application of nanoparticles in biomedical imaging and clinical diagnosis.[1–6] Before biomedical applications, they need to be refined to obtain good water solubility because most of them are water-insoluble and non-toxicity if they contain toxic elements *via* surface engineering.[7,8] Among nanoparticles, carbon-based nanomaterials such as carbon dots, carbon nanotubes, and nanodiamonds (NDs) have attracted great attention due to their relatively low toxicity as they are made of carbons.[9–11] Importantly, their attractive optical and magnetic properties may be useful for fluorescent imaging (FI) and magnetic resonance imaging (MRI) probes.[9–11]

In particular, NDs as a metastable allotrope of carbons are especially attractive owing to their strong sp^3 bonding structure, leading to superior chemical stability, inertness, and hardness.[12,13] Although their core is chemically stable and inert, their surface is composed of graphitic sp^2 carbons which can be easily conjugated with various functional molecules for biomedical applications.[14] Several researchers have developed surface homogenization methods such as carboxylation,[15] halogenation,[16] hydrogenation,[17] amination,[18] hydroxylation,[19] and graphitization.[20] These functional groups can be further conjugated with hydrophilic ligands,[21] peptides,[22] proteins,[23] nucleic acids,[24] drugs,[25] fluorescent dyes,[26] cancer targeting ligands,[27] dopamine derivatives,[28] and additional imaging probes,[29] which were conjugated directly or *via* linkers.[30–33] NDs can be introduced with nitrogen vacancy (NV) defects as color centers *via* irradiation of high-energy particles (p^+, He^+, or e^-) followed by high temperature annealing, making them promising candidates as FI probes.[34,35] NDs can also act as MRI probes after conjugation with Gd(III)-complexes or Mn(II)-complexes on ND surfaces, extending their functionality to powerful hybrid MRI and FI probes.[36–44] In addition, NDs themselves exhibit paramagnetic and ferromagnetic properties, which will be useful for use as MRI probes.[45] Taking all these attractive features together, NDs have emerged as promising FI and MRI probes in single or multi-modal biomedical imaging applications.[46]

Currently, various production methods of NDs have been developed; these are detonation,[47,48] fragmentation of high pressure and high temperature (HPHT) microdiamonds,[49,50] laser ablation,[51–53] chemical vapor deposition (CVD),[54–56] chlorination of carbides,[57] ultrasound cavitation,[58] ion beam irradiation of graphites,[59] and electron irradiation of carbon onions.[60] Among them, NDs produced by first two methods are most common and commercially available.[61,62] The first four production methods are briefly described in this review. Notably, the particle size and surface properties depend on the production method and thus, applications are somewhat tied to the production method.[63]

[a]*Department of Chemistry, College of Natural Sciences, Kyungpook National University, Taegu 41566, South Korea. E-mail: ghlee@mail.knu.ac.kr; Fax: +82-53-950-6330; Tel: +82-53-950-5340*
[b]*Department of Molecular Medicine, School of Medicine, Kyungpook National University, Taegu 41944, South Korea. E-mail: ychang@knu.ac.kr; Tel: +82-53-420-5471*

© 2023 The Author(s). Published by the Royal Society of Chemistry

Open Access Article. Published on 03 November 2023. Downloaded on 2/10/2026 5:30:09 AM. This article is licensed under a Creative Commons Attribution-NonCommercial 3.0 Unported Licence.

In this review, we concisely provided an insight into the recent advances in ND research such as the production and purification, surface homogenization and functionalization, physicochemical properties, biocompatibilities, and biomedical FI and MRI applications.

Production methods

Detonation

As shown in Fig. 1a,[64] NDs are produced through explosion of a mixture of 2,4,6-trinitrotoluene and 1,3,5-trinitroperhydro-1,3,5-triazine in the presence of a combined atmosphere of N_2, H_2O, and CO_2 in a metallic chamber. The explosion generates HPHT conditions ($P > 10$ GPa; $T > 3000$ K),[64] resulting in ND crystals (called detonation NDs) *via* condensation of supersaturated carbon vapors.[65,66] They consist of a ND core surrounded by a few layers of sp^2 carbons. Their particle diameters typically range from 1 to 10 nm,[65] with nearly spherical shape. However, they exhibit severe aggregations due to appreciable amount of sp^2 surface carbons. They possess low nitrogen impurities which are needed to generate NVs as color centers. The NDs can be purified through oxidation with strong liquid oxidants such as HCl/HNO_3, $HClO_4$, H_2SO_4/HNO_3, HF/HCl, $K_2Cr_2O_7/H_2SO_4$, and HNO_3/H_2O_2 (refs. [67] and 68) or with air or ozone at elevated temperatures (400–430 °C).[69–72] These oxidations introduce oxygen-containing groups on ND surfaces such as hydroxyl, carbonyl, and carboxyl groups. A high energy balling[73] or a salt-assisted ultrasonic de-aggregation[74–76] can be used to separate aggregated NDs into individual NDs; the latter method is preferred because the former method leaves broken ball materials after milling. In addition, annealing at 500 °C followed by centrifugation of NDs in aqueous colloidal solution can be used to obtain de-aggregated NDs by removing surface graphite carbons on ND surfaces;[77] even high-purity NDs of ~1 nm can be obtained by controlling annealing temperature, whereas the former two methods allow only de-aggregations of NDs.

Fragmentation of HPHT microdiamonds

As shown in Fig. 1b,[78] graphites or nanotubes or fullerenes as carbon source in a reactor chamber are brought to a high pressure (5–6 GPa) and high temperature (1300–1700 °C).[78] Iron and other metals such as cobalt and nickel as catalysts and small diamonds as crystallization seeds are provided. Under HPHT conditions achieved with a heater and carbide piston, carbon atoms are deposited on the diamond seed surfaces due to the temperature difference (20–50 °C) between the carbon source (high temperature side) and seed diamonds (lower temperature side) and exhibit transition from sp^2 to sp^3, making diamond seeds grow into bulk diamonds.[78] The obtained diamonds are fragmented into NDs with size of 2–50 nm *via* bead-assisted sonic disintegration or mechanical ball milling (the final fragmented diamonds are simply called HPHT NDs). Finally, impurities such as graphites and metals are eliminated *via* purification process.[79] Compared with detonation NDs, HPHT NDs have less amount of surface sp^2 carbons, leading to less aggregation, non-spherical shape with sharp edges, and higher nitrogen impurities.

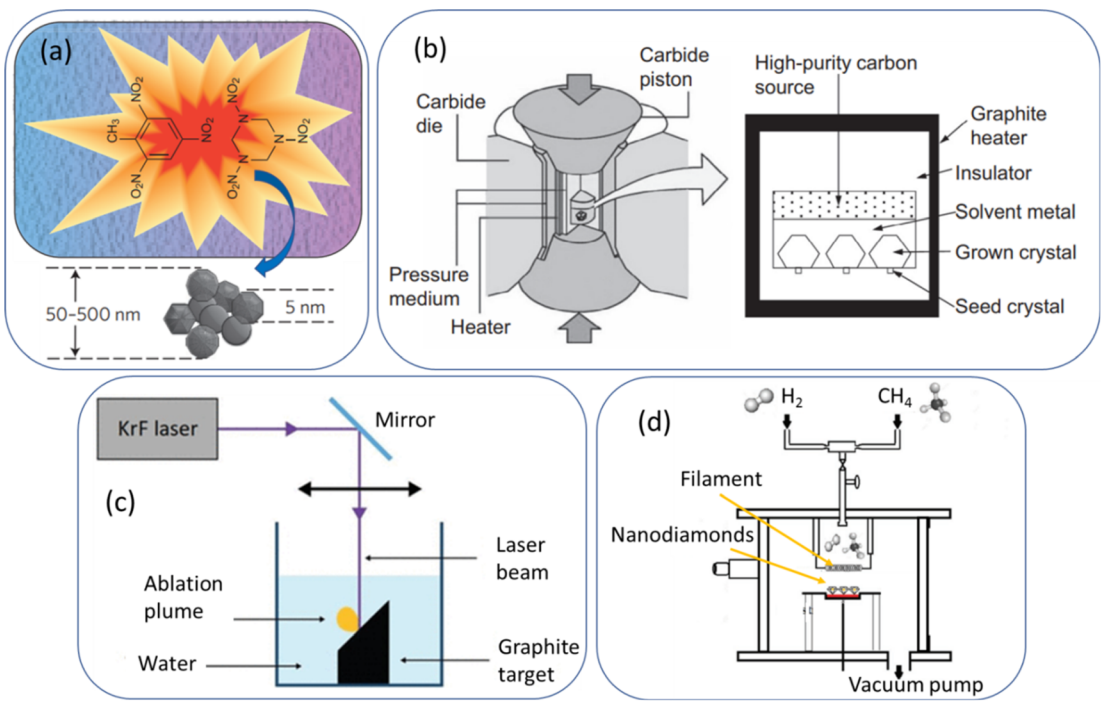

Fig. 1 (a) Detonation production of nanodiamonds,[64] (b) HPHT production of microdiamonds,[78] (c) laser ablation production of nanodiamonds,[53] and (d) CVD production of nanodiamonds.[55] Reproduced with permissions from ref. 64 Copyright 2012 Springer-Nature, ref. 78 Copyright 2016 Elsevier, and ref. 53 Copyright 2018 Springer.

© 2023 The Author(s). Published by the Royal Society of Chemistry

Open Access Article. Published on 03 November 2023. Downloaded on 2/10/2026 5:30:09 AM.
This article is licensed under a Creative Commons Attribution-NonCommercial 3.0 Unported Licence.

Laser ablation

As shown in Fig. 1c,[53] a pulsed laser beam is focused onto graphite target immersed in water.[51–53,80,81] The laser pulse leads to the vaporization of carbon atoms to the surrounding liquid in the form of an ablation plume. Carbon atoms trapped inside the bubble under HPHT conditions ($P = 1$–10 GPa; $T = 5000$–6000 K)[80] are subject to the formation of NDs with particle diameters of 3 to 15 nm[51] or ~100 nm,[81] depending on laser power conditions. This method is more environmentally green and less hazardous compared with detonation and HPHT methods. In addition, high purity NDs with minimal metallic impurities can be obtained.

CVD

As shown in Fig. 1d,[55] a ND thin film can be obtained from the decomposition of methane in an excess of hydrogen gas in a plasma reactor.[56,82] Jin-Woo *et al.* reported NDs of 4–6 nm using this method.[82] Depending on the relative concentration of the gas mixture (CH_4/H_2), microdiamonds (>100 nm), NDs (10–100 nm), and ultrasmall (<10 nm) NDs in a film can be produced.[56] For the synthesis mechanism of CVD NDs, a carbon-containing precursor (~1% CH_4 in H_2) is introduced into a reaction chamber and then, plasma (a mixture of $^{\bullet}H$ and $^{\bullet}CH_x$ radicals and electrons) is produced through microwave discharge or hot filament discharge.[56,83] The released carbon atoms from the precursors form diamond nuclei in gas phase or on a substrate, serving as templates for further diamond growth. In addition, NDs can grow on prepared diamond seeds on a substrate.[83] The diamonds grow slowly through the addition of carbon atoms onto the growing diamond lattice, ultimately yielding NDs.

Comparison between different production methods

For detonation NDs, Osswald *et al.* found that the as-prepared (*i.e.*, pristine) detonation NDs (d ~5 nm) contained 77% sp^2 carbons using soft X-ray absorption near-edge structure (XANES) spectroscopy, but after air oxidation, the amount of sp^2 carbons was reduced to 5%.[71] Stenclova *et al.* estimated 45% sp^2 carbons for as-prepared detonation NDs (d = ~5 nm) using high-resolution XPS.[84] Stehlik *et al.* prepared sub-10 nm HPHT NDs and estimated 52% sp^2 carbons for as-prepared HPHT NDs using XPS, but sp^2 carbons decreased to 9% after air oxidation at 450 °C for 1–2 h.[77] For CVD NDs, Kozakov *et al.* estimated 32–33% sp^2 carbons using XPS.[85] For laser ablation NDs, Xiao *et al.* produced NDs (3.1–3.6 nm) *via* laser ablation of coals and estimated 12% sp^2 carbons using XPS.[86]

Detonation NDs, HPHT NDs, and laser ablation NDs are produced under HPHT conditions and commercially available because they can be produced on a large scale at a reasonable cost. However, CVD NDs which are produced through nucleation reactions on a substrate, are not commercially available because the CVD synthesis takes a long time and thus, production cost is high.

Surface homogenization and hydrophilization

Surface homogenization

ND surfaces contain sp^2 carbons and a mixture of hydroxyl, carbonyl, and carboxyl groups after production and purification (Fig. 2).[87] Therefore, ND surfaces should be uniformly terminated with one type of functional groups to facilitate further conjugation with other ligands.[31,88,89] As shown in Fig. 2, the surface homogenization includes carboxylation, hydroxylation, halogenation, amination, hydrogenation, and graphitization.[87] Alternatively, silica can be coated on ND surfaces because the silica shell contains rich hydroxyl groups.[90,91] Namely, core@shell structure of NDs such as ND@silica in aqueous media may be also used for surface homogenization of NDs with numerous –OH groups on silica surfaces.[90,91]

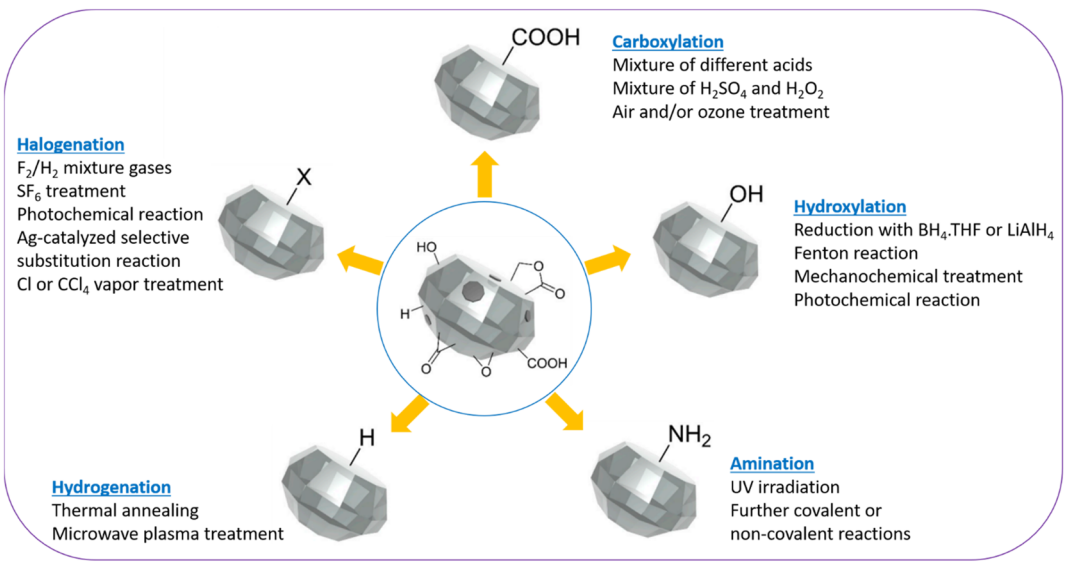

Fig. 2 Schematic representation of homogenization of ND surfaces *via* carboxylation, hydroxylation, hydrogenation, amination, and halogenation.[87]

Open Access Article. Published on 03 November 2023. Downloaded on 2/10/2026 5:30:09 AM.
This article is licensed under a Creative Commons Attribution-NonCommercial 3.0 Unported Licence.

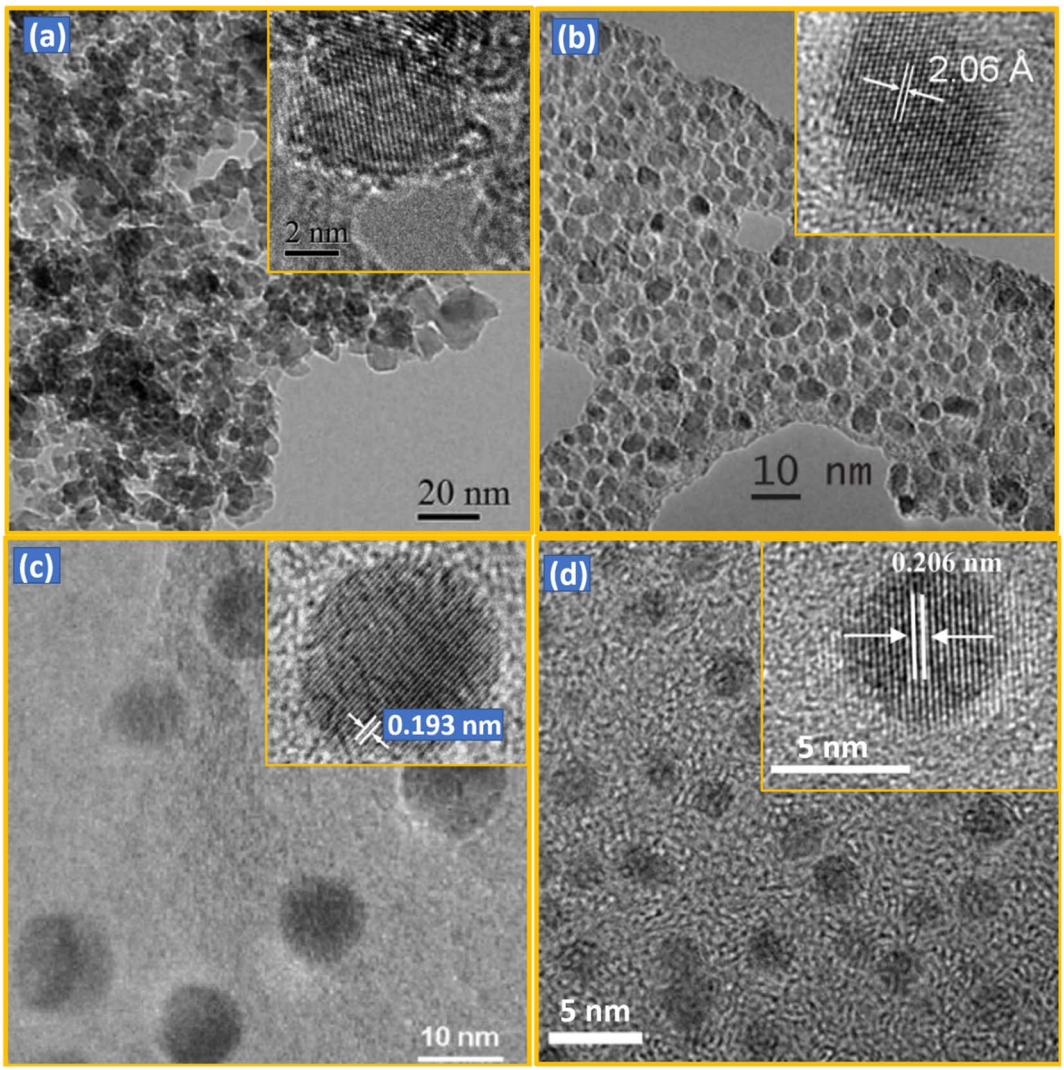

Fig. 3 TEM images of NDs synthesized by different methods: (a) detonation (d = 4–5 nm),[116] (b) HPHT after fragmentation (d = 2–7 nm; d_{avg} = 3.5 nm),[112] (c) CVD (d = 1–10 nm),[57] and (d) laser ablation (d_{avg} = 3.5 nm).[117] Low- and high (inset)-resolution images are provided. Reproduced with permissions from ref. 116 Copyright 2012 Royal Society of Chemistry, ref. 112 Copyright 2009 IOP Science, ref. 57 Copyright 2003 American Institute of Physics, and ref. 117 Copyright 2015 American Chemical Society.

Surface hydrophilization

Surface homogenized NDs are not colloidally stable in aqueous phase and thus, should be further grafted with hydrophilic polymers such as polyethylene glycol (PEG),[92,93] PEG derivatives,[94,95] polyglycerol,[39,96–98] polyethylenimine (PEI),[99] and polydopamine.[100] After this, hydrophilic polymer-grafted NDs can be further conjugated with diagnostic and therapeutic molecules for desired biomedical applications. ND–COOH can be conjugated with –NH_2 groups of hydrophilic polymers *via*

Table 1 Particle diameter, morphology, and application of NDs produced by various methods

Production method	Particle diameter[a]	Morphology	Application	Refs
Detonation	1–10 nm	Nearly spherical, aggregated	Lubrication, composite filler	64, 65, and 116
Fragmentation of HPHT microdiamond	2–50 nm	Irregular shape with sharp edges	Optical probe	78 and 112
CVD	4–6 nm, 10–100 nm, >100 nm	Nearly spherical	Coating, abrasive	56, 57, and 82
Laser ablation	3–15 nm, ~100 nm	Nearly spherical	Magnetic probe	51, 52, 81, and 117

[a] Particle diameter depends production method and conditions.

© 2023 The Author(s). Published by the Royal Society of Chemistry

Open Access Article. Published on 03 November 2023. Downloaded on 2/10/2026 5:30:09 AM.
This article is licensed under a Creative Commons Attribution-NonCommercial 3.0 Unported Licence.

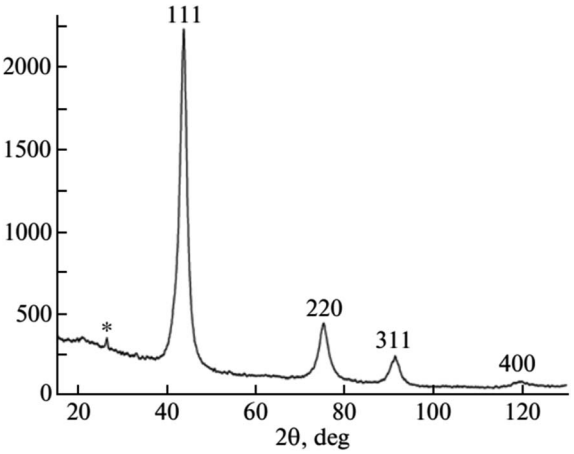

Fig. 4 XRD pattern of NDs produced by laser ablation (d = 3–4 nm).[114] Reproduced with permission from ref. 114 Copyright 2013 Springer.

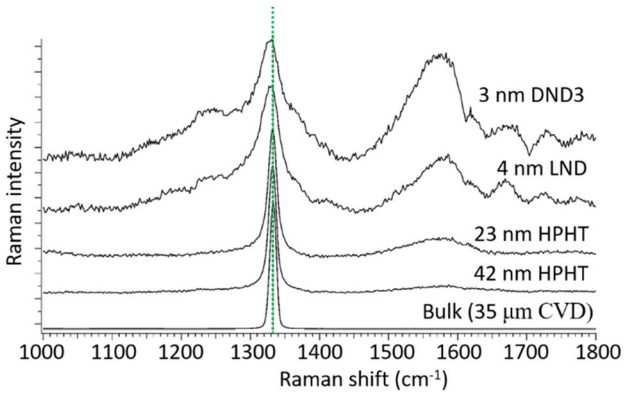

Fig. 5 Raman spectra of NDs of different sizes under 355 nm excitation. Size in this figure is estimated by dynamic light scattering (DLS) for HPHT and DND3 NDs and by XRD for the LND NDs. The peak at 1332.9 cm^{-1} is due to the C–C sp^3 chemical bond as indicated by the dotted line. The broad peak at ~1580 cm^{-1} is due to graphite carbons on ND surfaces, which becomes stronger for smaller NDs owing to their higher surface to volume ratios.[115] Reproduced with permission from ref. 115 Copyright 2017 Elsevier.

amide bond using 1-ethyl-3-(3-dimethylaminopropyl) carbodiimide (EDC)/*N*-hydroxysuccinimide (NHS) coupling reaction.[101–103] Or ND–COOH can be activated with thionyl chloride ($SOCl_2$) to form acyl chloride, *i.e.*, ND–COCl, which can directly react with amines of hydrophilic polymers to form amide bond.[104–107] ND–NH_2 can be conjugated with –COOH groups of hydrophilic polymers *via* amide bond using EDC/NHS coupling reaction.[108–110] ND–OHs can be conjugated with acid chloride (ClO^-) groups of hydrophilic polymers to form ester bond, *i.e.*, ND–OOC–polymer[111] or with silanes to form ND–O–Si–polymer.[31] Silica coating can be considered as another method of surface hydrophilization of NDs.[90] This is because silica and terminal –OH groups are hydrophilic. Bumb *et al.* used tetraethyl orthosilicate as silica precursor to obtain ND@silica in aqueous media,[90] which was stable whereas uncoated NDs precipitated in aqueous media.

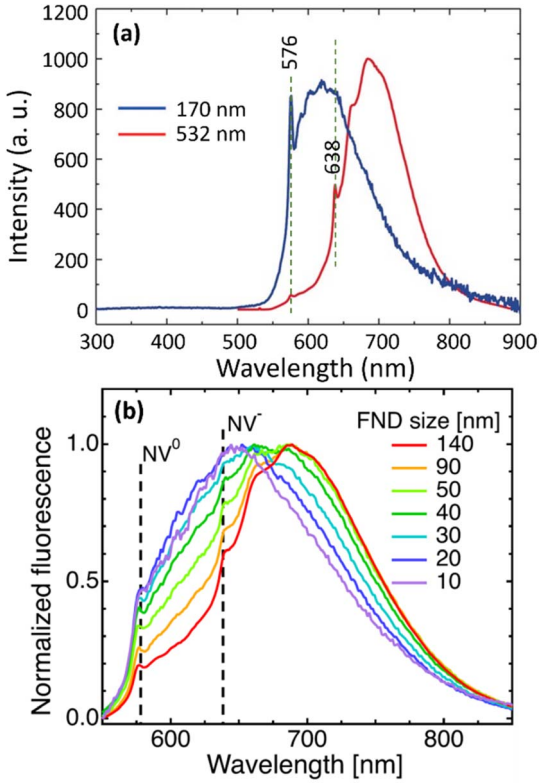

Fig. 6 (a) Photoluminescence (PL) spectra of 100 nm HPHT NDs at 300 K with excitation wavelengths of 170 nm synchrotron source and 532 nm laser light, showing zero-phonon lines (ZPL) at 576 and 638 nm for NV^0 and NV^- centers, respectively.[133] Vertical dotted lines indicate ZPL positions. (b) PL spectra as a function of HPHT ND diameters, showing no dependence of NV^0 and NV^- center positions on particle diameter (510 nm laser excitation).[122] Reproduced with permissions from ref. 122 Copyright 2019 IOP Science and ref. 133 Copyright 2017 Wiley.

Physicochemical properties

NDs can be characterized with various techniques.[112–117] As shown in low- and high (inset)-resolution transmission electron microscope (TEM) images in Fig. 3a–d and Table 1, the diameters of NDs largely depend on production method. The detonation NDs contain a nearly spherical shape in severely aggregated forms with thick graphitic shell.[64,65,116] NDs obtained *via* fragmentation of HPHT microdiamonds (simply, HPHT NDs) have irregular shapes with sharp edges, but are well dispersed.[78,112] CVD NDs[56,57,82] and laser ablation NDs[51,52,81,117] are nearly spherical and well dispersed. The particle diameters of detonation NDs are very small (d_{avg} = 5 nm) and narrow (2–9 nm)[65] (polydispersity index, PDI = 0.11–0.13).[3] The particle diameters of HPHT NDs range from 2 to 50 nm, showing a broad size distribution because they are produced from fragmentation of HPHT microdiamonds.[112] Laser ablation NDs exhibit the particle diameters of 3 to 15 nm[51,52] or ~100 nm,[81] depending on laser power conditions. CVD diamonds exhibit microdiamonds (>100 nm), NDs (10–100 nm), and ultrasmall (<10 nm) NDs, depending on the relative concentration (CH_4/H_2).[91]

Open Access Article. Published on 03 November 2023. Downloaded on 2/10/2026 5:30:09 AM.
This article is licensed under a Creative Commons Attribution-NonCommercial 3.0 Unported Licence.

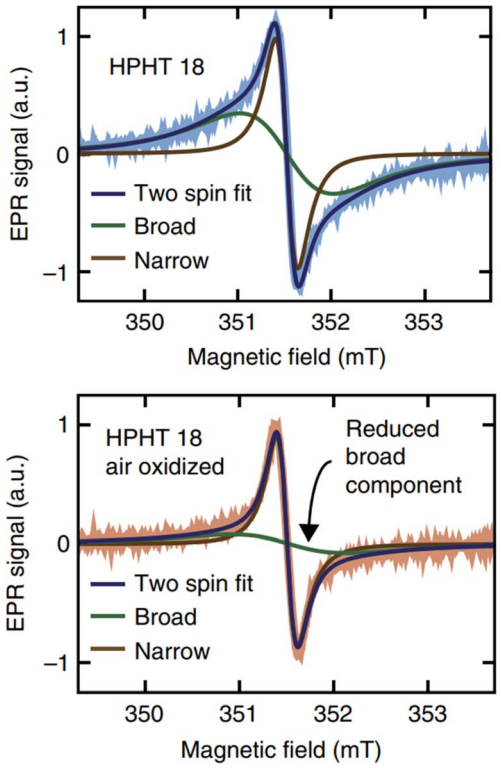

Fig. 7 The top shows EPR spectra of HPHT 18 nm NDs in deionized water and the bottom shows the EPR spectra of the same NDs after air oxidation. Air oxidation removed the broad component arising from disordered dangling bonds at the ND surfaces while leaving the narrow component arising from lattice defects in the crystalline core unaffected.[45] Reproduced with permission from ref. 45 Copyright 2017 Springer-Nature.

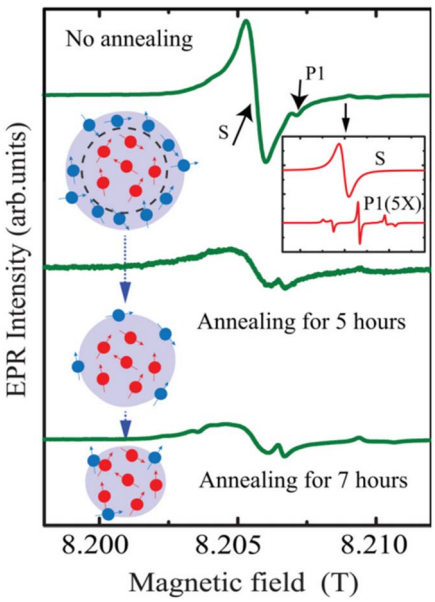

Fig. 8 EPR analysis of 50 nm NDs before and after air annealing for 5 and 7 h. The inset on the top right shows contributions of nitrogen impurity centers (labeled as P1) and surface spins (labeled as S) to the EPR spectra. The EPR spectra under the annealing process are shown below. The red dots in the drawing represent the P1 centers and the blue dots represent surface spins.[143] Reproduced with permission from ref. 143 Copyright 2020 American Institute of Physics.

NDs have a sp^3 bonding structure. As observed in the X-ray diffraction (XRD) patterns (Fig. 4),[114] NDs exhibit a face-centered cubic structure with the major peak at 2θ of 44° from the (111) diffraction plane along with two other peaks at 2θ of 75° and 91° from the (220) and (311) diffraction planes, respectively. The broad peaks are owing to small particle sizes of NDs.[113,114]

The Raman spectra of NDs produced by different methods exhibit a diamond peak from the C–C sp^3 chemical bond at 1332.9 cm^{-1} (Fig. 5).[115] The broad peak at ~1580 cm^{-1} is due to graphite carbons on ND surfaces, which becomes stronger for smaller NDs owing to their higher surface to volume ratios.

The polydispersity index (PDI) of NDs defined as $(\sigma/d)^2$ (σ = standard deviation of particle diameter distribution and d = average particle diameter) can be measured using a TEM or a dynamic light scattering (DLS) instrument.[118] The DLS-PDI is more commonly used than TEM-PDI because DLS-PDI can be obtained from DLS. The DLS-PDI values of NDs synthesized by different methods are as follows. The detonation NDs exhibited PDI values ranging from 0.1 to 0.6,[33,119] HPHT NDs[32] and CVD NDs[120] exhibited PDI values ranging from 0.1 to 0.3, and laser ablation NDs provided PDI values of 0.5 after glycidol surface coating.[121] It should be noted that the PDI values are subject to variation based on experimental conditions and post-synthesis treatments.

Wilson *et al.* investigated stability of HPHT NDs in water and biological media such as 10% fetal bovine serum (FBS) in water, Dulbecco's modified eagle medium (DMEM; common cell culture medium), and DMEM with the addition of 10% v/v FBS (simply denoted as CM).[122] 1% antibiotic penicillin–streptomycin was added to both DMEM and CM media. DLS was used to investigate stability of NDs in water and biological media as a function of time. Hydrodynamic diameter did not change in water with time, only slightly increased in FBS and CM media with time, but severely increased in DMEM with time, resulting in precipitation of NDs owing to ND aggregation; therefore, stability of NDs in water, FBS, and CM was good, but poor in DMEM.

The surface zeta potential of NDs is important for colloidal stability in solution. The surface zeta potential of as-synthesized detonation NDs was slightly positive (~1.5 mV) owing to –OH groups on the ND surfaces.[123] However, surface zeta potential of detonation NDs became highly positive (>20 mV) or highly negative (<−20 mV) after surface modifications with different type of acids, respectively.[124] On the other hand, the surface zeta potential of as-prepared HPHT NDs was highly negative (<−40 mV) owing to –COOH groups on the ND surfaces,[125,126] but became positive after successive heat treatments in air (480 °C, 5 h), vacuum (0.001 mbar, 1000 °C, 2 h), and H_2 (500 °C, 10 mbar, 5 h).[126]

Fluorescent properties

Color centers are crystal defects that absorb and emit photons while the crystal itself has no absorption; *i.e.*, ND itself is colorless and transparent. The fluorescence of NDs is due to

© 2023 The Author(s). Published by the Royal Society of Chemistry

Open Access Article. Published on 03 November 2023. Downloaded on 2/10/2026 5:30:09 AM.
This article is licensed under a Creative Commons Attribution-NonCommercial 3.0 Unported Licence.

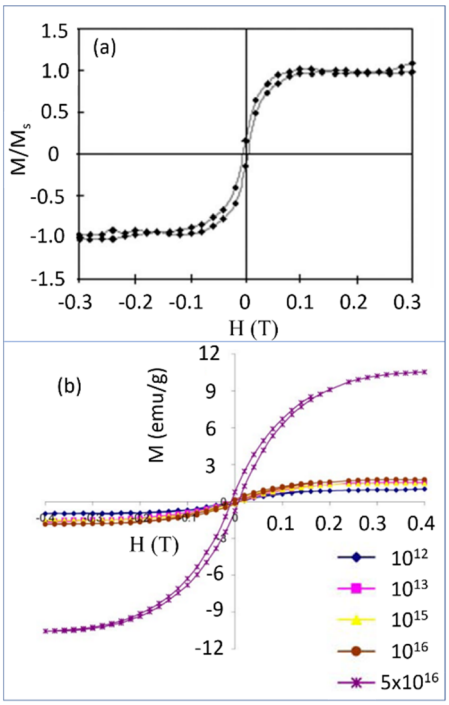

Fig. 9 (a) Magnetization (M) *versus* applied field (H) curves for the detonation NDs ($d = 4–5$ nm) (M_s = saturation magnetization) with ^{15}N dose at (a) 5×10^{14} cm^{-2} and (b) various doses: enhanced magnetizations were observed with doses above 5×10^{16} cm^{-2}.[144] Reproduced with permission from ref. 144 Copyright 2005 American Physical Society.

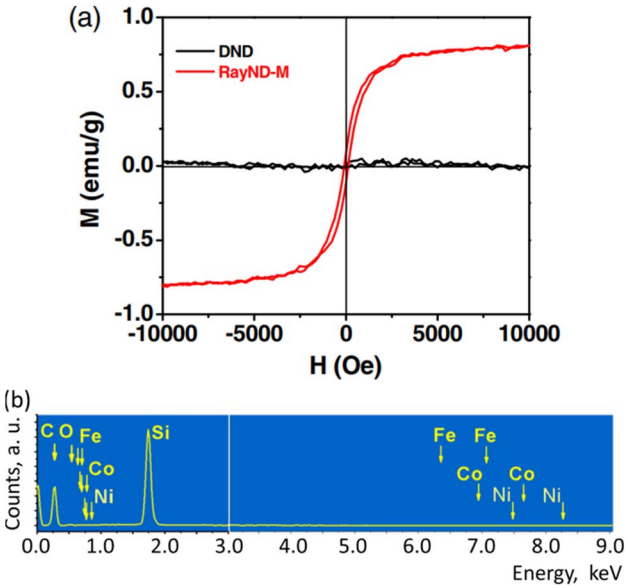

Fig. 10 Magnetic properties of RayND-M ($d = 4.3–4.5$ nm). (a) Magnetization curve of RayND-M [in comparison with ordinary detonation ND (DND), $d = 3–10$ nm]. (b) EDS spectrum of RayND-M; Fe, Co, and Ni atoms as impurities were not detected.[139] Reproduced with permission from ref. 139 Copyright 2018 SPIE.

impurity atoms such as N and Si (mostly N) bound to structural vacancies. The most common color centers are the NVs which are created by irradiating NDs with high-energy particles (p^+, He^+, or e^-), followed by vacuum annealing of NDs at high temperatures (600–800 °C);[127–129] vacancies are first produced by irradiation and impurity atom vacancy centers are produced from migration of impurity atoms to the vacancies during heat treatment. Two types of NV centers are produced; neutral (NV^0) emitting visible photons with slightly shorter wavelengths at 576 nm compared with those of negatively charged (NV^-) emitting red photons;[130–132] NV^- centers are dominant at 638 nm and their quantum yield is ~1.0. In addition, conjugation of octadecylamine to NDs allowed blue photon emissions.[104]

Fig. 6a shows PL spectra of 100 nm HPHT NDs, showing two emissions, *i.e.*, zero-phonon lines (ZPL) of NV^0 and NV^- centers at 576 and 638 nm, respectively; they were obtained with excitation wavelengths of 170 nm synchrotron far-UV source and 532 nm laser light, respectively.[133] In addition, the positions of NV^0 and NV^- centers do not change with particle diameters whereas broad emission from graphitic carbons on ND surfaces are red-shifted with increasing ND size, as shown in Fig. 6b.[122]

Moreover, since the NV centers are incorporated deeply inside the ND matrix, their optical properties are not altered by surface coating.[90,134,135] The exceptional photostability with no photobleaching of NV centers in NDs provides a greater advantage to emerge as an ideal candidate for long term imaging.[131] Most brightly fluorescent NDs have been made from HPHT NDs because the HPHT NDs contain the highest amount of nitrogen impurities with a typical concentration of 100–200 ppm among NDs produced with different methods.[112,127] A recent study showed that NV centers in detonation NDs can be enhanced up to 10^4 ppm through a HPHT sintering.[136]

NDs can be engineered to emit near-infrared fluorescence (NIRF). This property makes them useful in bio-imaging applications because NIR light can penetrate deeply into biological tissues. One of the commonly employed methods to induce NIRF in NDs is the introduction of silicon vacancy (SiV)

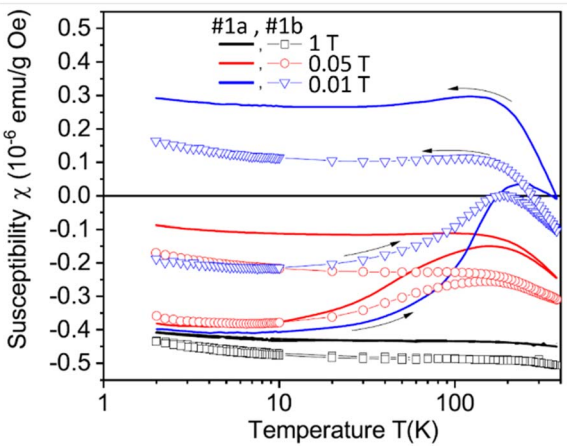

Fig. 11 Zero-field-cooled and field-cooled curves of the CVD samples (#1a: samples after the laser-cut and #1b: after laser-polishing of the laser-cut surface) as a function of temperature between 2 and 380 K at applied fields of 0.01, 0.05, and 1 T.[145]

Open Access Article. Published on 03 November 2023. Downloaded on 2/10/2026 5:30:09 AM. This article is licensed under a Creative Commons Attribution-NonCommercial 3.0 Unported Licence.

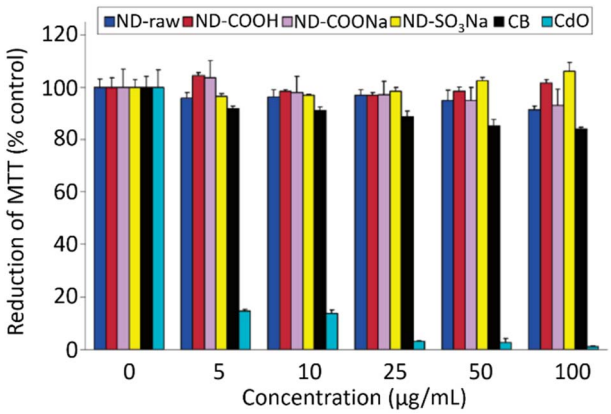

Fig. 12 Cytotoxicity of neuroblastoma cells incubated with various types of NDs (d = 2–10 nm), carbon black (CB) nanoparticles (d = 20–30 nm), and CdO nanoparticles (submicrometer size) *via* MTT assay.[150] Reproduced with permission from ref. 150 Copyright 2007 American Chemical Society.

centers (zero phonon line center = 738 nm) into NDs.[137,138] The SiV centers are created by introducing silicon precursors as impurities into the diamond growth region for HPHT diamonds[137] or detonation region for detonation NDs.[138]

Paramagnetic and ferromagnetic properties

Bulk diamonds are diamagnetic owing to sp^3 bonding structure. However, NDs can take paramagnetic or ferromagnetic properties.[139] Paramagnetism comes from graphitic surface layers in NDs.[140] Shames *et al.* found a high concentration of radical like-paramagnetic surface spins (10^{20} spins per g).[141,142] Fig. 7 shows electron paramagnetic resonance (EPR) spectra of 18 nm HPHT NDs showing that air oxidation of NDs reduces the amplitude of the broad component in the spectra owing to the removal of paramagnetic surface spins at the ND surfaces.[45] A similar thing was observed in 50 nm NDs; *i.e.*, the paramagnetic component from nitrogen impurity centers in ND crystalline core did not change during annealing while that from surface spins were significantly removed (Fig. 8).[143]

The ferromagnetism in NDs is not clearly understood up to now. Talapatra *et al.* observed ferromagnetism after they irradiated NDs with ^{15}N and ^{12}C ions; the results for ^{15}N ion irradiation are provided in Fig. 9a and b.[144] At low doses, the magnetization was independent of the irradiating species indicating that it mainly arises from structural deformation (*i.e.*, generating sp^2/sp^3 defect structures) of the carbon bonds in NDs. However, ^{15}N implants exhibited higher saturation magnetizations than ^{12}C implants at higher doses (*i.e.*, 5×10^{16} cm^{-2} in Fig. 9b whereas the magnetization was independent of the irradiating species up to 10^{16} cm^{-2} doses), which could be due to extensive defect generation or graphitization and, to some extent, incorporation of nitrogen in the graphitic network and formation of C–N bonds. Perevedentseva *et al.* prepared ferromagnetic NDs *via* thermal treatment of NDs produced by laser ablation in liquid (called RayND-M).[139] They demonstrated

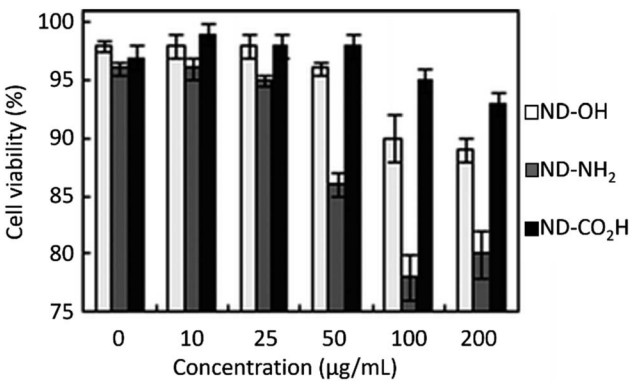

Fig. 13 Cell cytotoxicity of NDs (d_{avg} = 4 nm) on HEK293 cells after normalization with respect to control cells that were not incubated with NDs. The control cells exhibited a cell viability of 97 ± 1% 24 h after incubation.[153] Reproduced with permission from ref. 153 Copyright 2010 Royal Society of Chemistry.

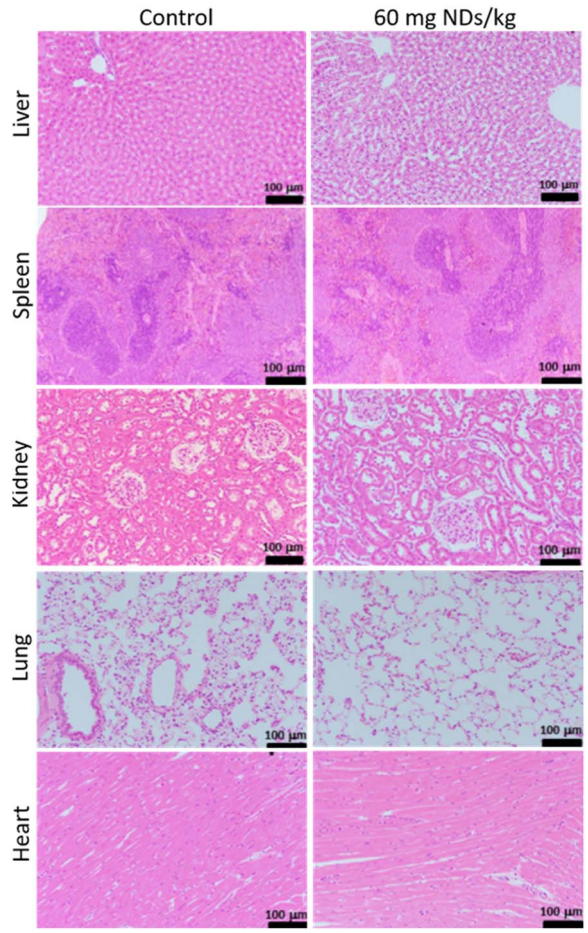

Fig. 14 Histopathology of rats showing no toxicity of NDs 12 weeks after intravenous injection of NDs (hydrodynamic diameter = 800 nm) and 8 weeks after intravenous injection of PBS solution (control). Images of hematoxylin- and eosin-stained liver, spleen, kidney, lung, and heart. N = 3 for all groups. Injection dose (2 mL of PBS for control rats; 60 mg NDs per kg rat).[162]

© 2023 The Author(s). Published by the Royal Society of Chemistry

Open Access Article. Published on 03 November 2023. Downloaded on 2/10/2026 5:30:09 AM. This article is licensed under a Creative Commons Attribution-NonCommercial 3.0 Unported Licence.

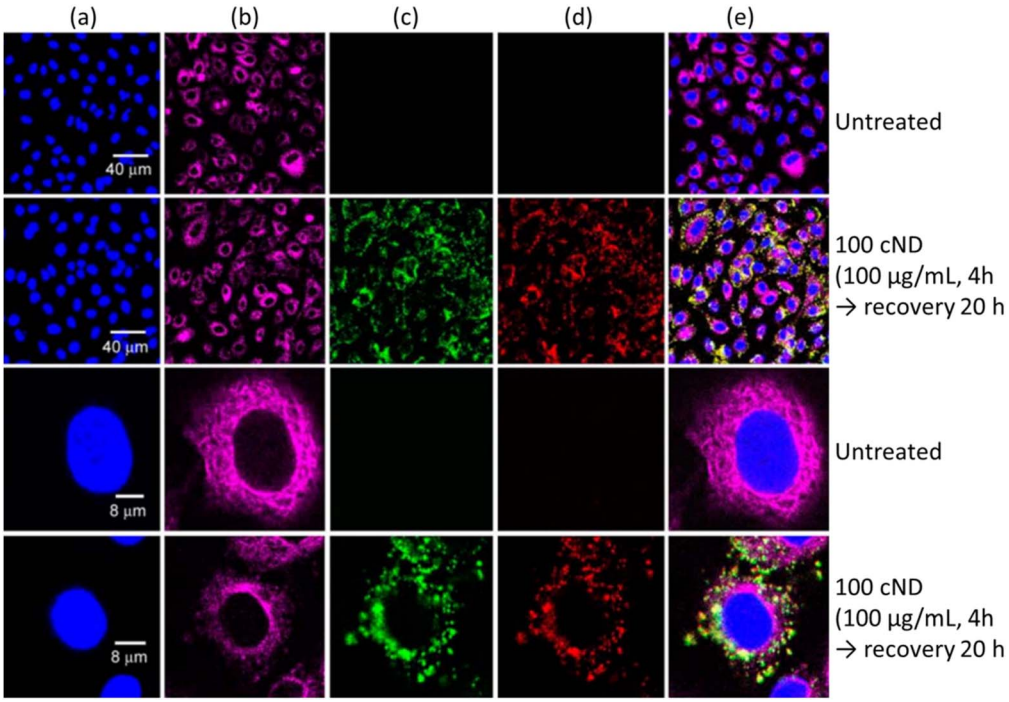

Fig. 15 Laser scanning confocal fluorescence images of A549 cells. (a) The cell nuclei were dyed with Hoechst 33 258 to show the nucleus position (Ex: 351 nm, Em: 350–460 nm). (b) The cell tissue was dyed with anti-β-tubulin (Cy3) to show the cell cytoskeleton (Ex: 543 nm, Em: 550–615 nm). The cells treated with 100 nm NDs with excitation with (c) 488 nm (Em: 500–530 nm) and (d) 633 nm (Em: 640–720 nm). (e) Overlaid images of (a)–(d).[170] Reproduced with permission from ref. 170 Copyright 2007 CellPress.

that the surface structural modification could be the source of ferromagnetism in RayND-M (Fig. 10a) rather than elemental contents (Fe, Co, and Ni) as impurities because no such metals were detected from elemental analysis using energy dispersive X-ray spectroscopy (EDS) (Fig. 10b). For comparison, detonation NDs did not exhibit ferromagnetism (Fig. 10a).

Setzer *et al.* investigated magnetic properties of natural and CVD diamonds after laser-cut.[145] All of them exhibited ferromagnetism after laser-cut owing to surface graphite formation on diamond surfaces. The surface graphites formed on CVD diamond surfaces were <20 nm thick after laser-cut and reduced by 10% after laser polishing of the laser-cut surface. The zero-field-cooled (ZFC) and field-cooled (FC) magnetization curves of the laser-cut CVD diamonds before (sample #1a) and after laser polishing of the laser-cut surface (sample #1b) were measured at 0.01, 0.05, and 1 T applied fields between 2 and 380 K as shown in Fig. 11. The observed saturation magnetization values were 10 to 20 emu g^{-1} at 300 K, similar to those obtained with pure graphites, supporting that the ferromagnetism of NDs resulted from surface graphites formed on ND surfaces by laser-cut.

In vitro and *in vivo* biocompatibility

NDs are considered to be the most biocompatible form among carbons (fullerene, graphene, carbon nanotubes, and so on).[146–151] The sp^3 carbon core of NDs is chemically inert and non-toxic. Therefore, toxicity of the NDs mostly comes from surface materials including sp^2 graphite carbons, functional groups, and metal impurities.[152–156] NDs did not show any noticeable toxicity on human embryonic kidney tumor (HEK293T) cells up to concentration of 400 μg mL^{-1} [concentration (μg mL^{-1}) = mass of NDs (μg)/volume of solution (mL)], confirming their non-toxicity.[131] The viability of neuroblastoma cells after incubation with various concentrations of various types of NDs, carbon black (CB) nanoparticles, and cadmium oxide (CdO) submicroparticles were assessed using 3-(4,5-dimethylthiazol-2-yl)-2,5-diphenyltetrazolium bromide (MTT) colorimetric assay (Fig. 12).[150] The results exhibit that all NDs are non-toxic and less toxic than CB whereas CdO submicroparticles are highly toxic. The cellular toxicity of NDs on human embryonic kidney 293 (HEK293) cells was ranked in the order of ND-NH_2 > ND-OH > ND-CO_2H at a concentration of 200 μg mL^{-1} (Fig. 13),[153] indicating that higher negative ND surface charges induce less cytotoxicity owing to less interaction between cells and NDs. Generally, large NDs (more than 100 nm) are more biocompatible than smaller NDs (5 nm).[157] This is due to more active surface materials of smaller NDs compared with those of large NDs.

The clearance of NDs from the body depends on their particle diameter and surface properties. Small NDs (d < 3 nm) grafted with zwitterionic molecules can be excreted from the body through the renal system,[158–160] whereas large NDs (d > 3 nm) grafted with polymers mostly accumulate in the body. NDs (d < 3 nm) may be excreted through the renal system within 1 h because inulin (3 nm) achieved 100% renal excretion with a blood half-life of only 9 min.[158] However, large NDs (d > 3 nm)

Open Access Article. Published on 03 November 2023. Downloaded on 2/10/2026 5:30:09 AM.
This article is licensed under a Creative Commons Attribution-NonCommercial 3.0 Unported Licence.

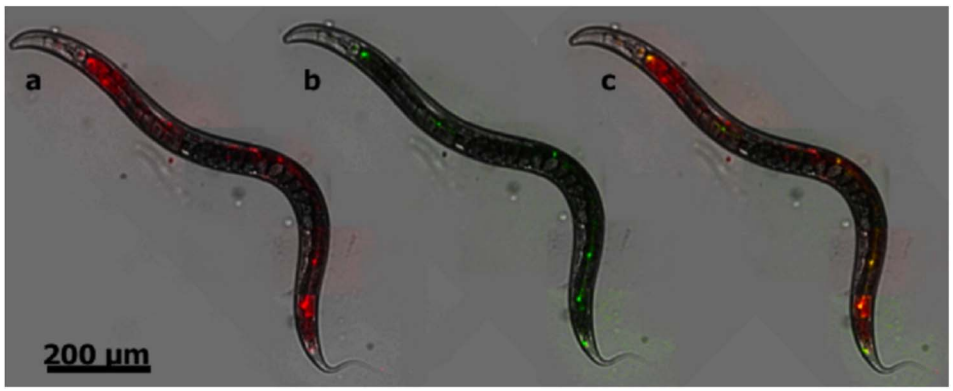

Fig. 16 Bright-field fluorescence merged images of *C. elegans* fed with NDs (d = 50 nm) with nitrogen vacancy centers. (a) A conventional fluorescence image obtained without SIP as shown in red, resulting from background and NDs. (b) An image obtained by SIP as shown in green, resulting from only NDs. (c) The merged image of a and b; fluorescence from NDs is given in yellow whereas that from other sources remains red.[171] Reproduced with permission from ref. 171 Copyright 2012 American Chemical Society.

are mostly taken up by the reticuloendothelial system (RES), particularly in the liver and spleen, followed by the excretion through the hepatobiliary system.[158] The excretion through the hepatobiliary system takes a long time. Yuan *et al.* investigated the biodistribution and fate of very large NDs (d = 50 nm) *in vivo*.[161] They found that approximately 60% of injected NDs were entrapped in the liver and 8% in the lung at 30 min after intravenous injection in mouse. These accumulation values remained for 28 days after injection, implying that large NDs are not or negligibly excreted from the body.

Barone *et al.* conducted an *in vivo* histological evaluation of various rat organs including the liver, spleen, kidney, lung, and heart 12 weeks after intravenous injection of large NDs (hydrodynamic diameter = 800 nm) (Fig. 14).[162] The analysis showed few changes in liver, spleen, kidney, lung, and heart after injection (60 mg of NDs per kg rat), showing no-toxicity of the NDs. All these *in vitro* and *in vivo* studies confirm that NDs are non-toxic.

Moore *et al.* conducted a comprehensive study on the biocompatibility of detonation NDs (hydrodynamic diameter = 52.7–59 nm) in non-human primates (*i.e.*, monkeys) for 6 months and rats for 2 weeks by analyzing urine, body weight, histology, and blood.[163] They did not find any adverse effects on various organs such as the liver, kidneys, and lung. This result supports the outstanding biocompatibility of NDs.

However, long-term toxicity (>1 year) of NDs should be carefully studied for clinical applications. For example, blood samples can be drawn and analyzed to detect any biomarkers that are indicative of potential inflammatory responses. In addition, routine welfare checks should be performed to monitor changes to the overall physical and mental health such as body weight, behavior, and signs of weakness of the animals. Furthermore, major organs should be collected and subjected to extensive histological analyses to detect any phenotypic changes.[164] These long-term toxicity data are essential for U.S. Food and Drug Administration (FDA) approval for clinical applications.[165]

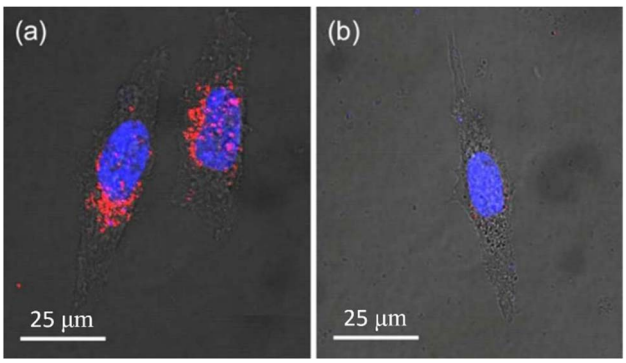

Fig. 17 Confocal microscopy fluorescence images of HeLa cells 2 h after incubation (d = ~100 nm; 25 μg mL^{-1}; 488 nm excitation) with (a) rA27-NDs and (b) rDA27-NDs as control. The red fluorescence in (a) is from targeted NDs, whereas negligible red fluorescence in (b) is owing to negligible targeting of NDs. The blue emission is due to fluorescence from Hoechst 33 342-stained cell nuclei.[174] Reproduced with permission from ref. 174 Copyright 2017 American Chemical Society.

Specific functionalizations

There are many studies on specific functionalizations of NDs by conjugating specific ligands to NDs. Lake *et al.* synthesized Nup98 antibody-conjugated NDs to target Nup98, a component of the nucleoporin ring structures of the nuclear pore complex (NPC).[166] The successful targeting of the Nup98 antibody-conjugated NDs onto the Nup98 of NPC was confirmed from TEM images and fluorescence imaging of NV centers of NDs. Leung *et al.* conjugated NDs with three ligands, *i.e.*, an antisense oligonucleotide ANA4625, a human immunodeficiency virus TAT protein, and a nuclear localization signal (NLS) peptide in series in aqueous media.[167] The ANA4625-NLS-TAT-NDs targeted the NPC and penetrated into cancer cells. They confirmed nuclear targeting through fluorescence imaging of NV centers of NDs. Nie *et al.* conjugated NDs with pH sensitive dextran to facilitate endocytosis of NDs inside HeLa cancer cells. They demonstrated cell internalization of NDs through fluorescence imaging of NV centers of NDs.[168]

© 2023 The Author(s). Published by the Royal Society of Chemistry

Open Access Article. Published on 03 November 2023. Downloaded on 2/10/2026 5:30:09 AM. This article is licensed under a Creative Commons Attribution-NonCommercial 3.0 Unported Licence.

Biomedical imaging applications

FI

NDs are emerging as a new and promising imaging agent for long term *in vitro* and *in vivo* studies.[34] NDs have defects as color centers that can emit fluorescence. ND fluorescence from NV centers is highly photostable with no photobleaching and quenching owing to protection by the robust diamond lattice.[131,169] Chao *et al.* successfully observed fluorescence emission from NDs treated into human lung epithelial (A549) cells (Fig. 15), confirming potential of NDs as imaging agents.[170] Igarashi *et al.* developed a background-free selective imaging protocol (SIP) to observe fluorescent NDs with nitrogen vacancy centers.[171] To this end, they irradiated microwave (2.87 GHz) to remove autofluorescence intensity from biological molecules. Using this imaging technique, they observed background-free fluorescence from NDs fed into *Caenorhabditis* (*C.*) *elegans* (Fig. 16).

NDs can be used as *in vivo* tracking nanoprobes utilizing their fluorescence properties of NV centers. Mohan *et al.* found that the NDs (hydrodynamic diameter = ~120 nm) enabled continuous imaging of the whole digestive system of the *C. elegans via* fluorescence imaging for several days after feeding them with NDs.[172]

NDs can be used as specific imaging agents after conjugation of specific targeting ligands with NDs. Han *et al.* synthesized hyaluronate (HA)-conjugated NDs (d = ~100 nm) to use them for *in vitro* human liver cancer cell (HepG2) imaging and *in vivo* liver imaging utilizing the fact that the liver cells possess abundant HA receptors.[173] Pham *et al.* synthesized rA27(aa 21–84)-conjugated NDs (d = ~100 nm) to use them for human HeLa cancer cell imaging.[174] As shown in Fig. 17a, rA27-conjugated NDs exhibited red fluorescence owing to their targeting to the glycosaminoglycans (GAGs) of HeLa cells, whereas rDA27-conjugated NDs as control showed negligible red fluorescence as shown in Fig. 17b because rDA27 is not specific to GAGs.

MRI

The paramagnetic and ferromagnetic properties of NDs are the potential sources for MRI. So far only the paramagnetic properties of NDs had been applied to MRI. Waddington *et al.* explored the Overhauser effect based on a proton–electron polarization transfer technique for MRI (called Overhauser-enhanced MRI: OMRI).[45] This effect transfers spin polarization from paramagnetic impurities (*i.e.*, NVs and unpaired electrons in sp^2 graphite shell) in NDs to ^{1}H proton spins in the surrounding water solution, creating MRI contrasts.[45] As shown in phantom images (Fig. 18a–d), higher contrasts were observed with increasing ND concentration in solution at 6.5 mT MR field, demonstrating the capability of NDs as imaging probes in MRI.[45] The same group applied the hyperpolarized ^{13}C (1.1% natural abundance carbon content in ND) to MRI *in vivo* at 7 T MR field.[175] They prepared hyperpolarized ^{13}C NDs using a 2.88 T superconducting nuclear magnetic resonance (NMR) magnet. An MR contrast image was clearly observed in mouse after intrathoracic injection of hyperpolarized 2 μm-diamonds dispersed in water, as shown in Fig. 18e.

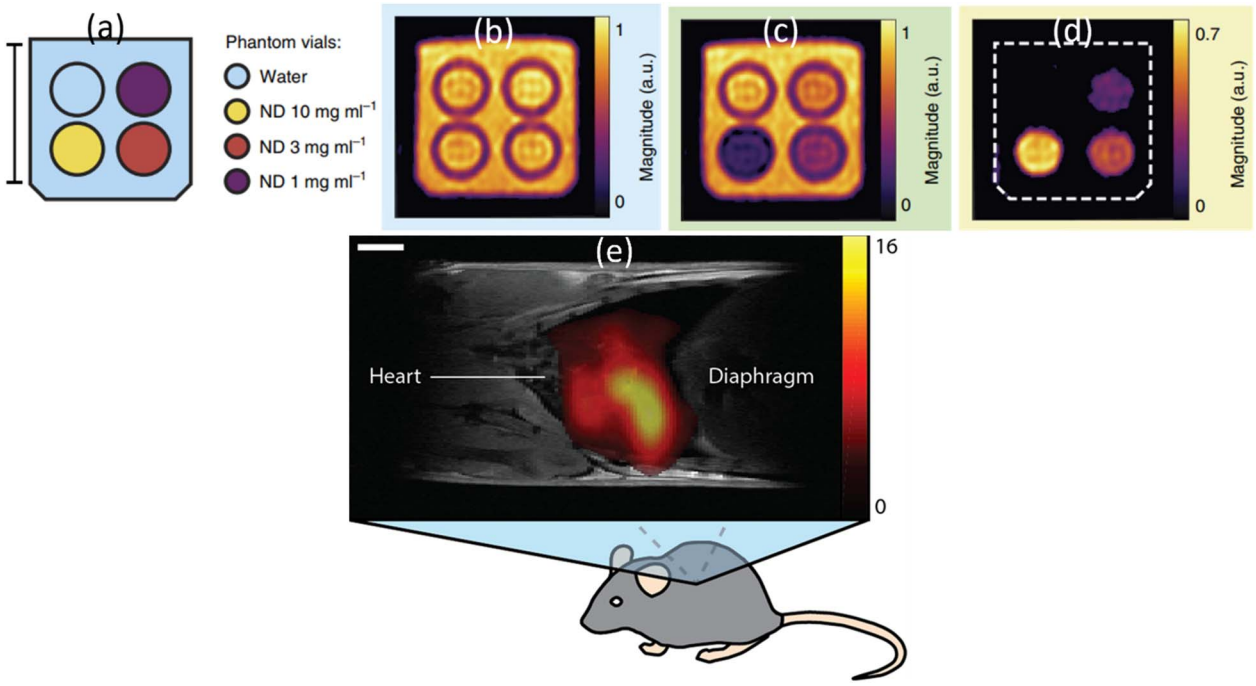

Fig. 18 OMRI at 6.5 mT MR field. (a) A vial of deionized (DI) water (blue) and vials containing 18 nm HPHT NDs at concentrations of 10 mg mL^{-1} (yellow), 3 mg mL^{-1} (red) and 1 mg mL^{-1} (purple). The surrounding volume was filled with DI water (blue). Scale bar is 20 mm. (b) Phantom image obtained *via* standard balanced steady-state free precession (bSSFP) MRI. (c) OMRI bSSFP phantom image. (d) The difference between b and c.[45] (e) A ^{1}H:^{13}C MR image at 7 T MR field for a mouse thorax after intrathoracic injection of hyperpolarized 2 μm diamonds. ^{1}H MRI was used for mouse imaging and ^{13}C MRI was used for hyperpolarized ND imaging: the scale bar is 3 mm.[175]

Open Access Article. Published on 03 November 2023. Downloaded on 2/10/2026 5:30:09 AM.
This article is licensed under a Creative Commons Attribution-NonCommercial 3.0 Unported Licence.

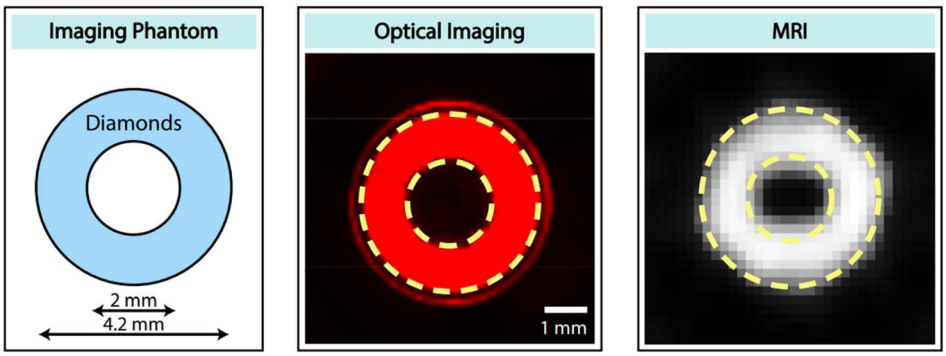

Fig. 19 Dual-modal optical and ^{13}C MR imaging. (left) Ring-shaped phantom filled with 40 mg of 200 μm diamonds. (middle) Fluorescence image with a 630 nm filter. (right) ^{13}C MR image.[176] Reproduced with permission from ref. 176 Copyright 2021 National Academy of Sciences USA.

Recently, Lv *et al.* reported that microdiamonds containing NVs can be used as dual-modal optical and ^{13}C MR imaging.[176] They used 40 mg of 200 μm diamonds for phantom imaging and successfully performed dual optical and MR imaging, as shown in Fig. 19.

Conclusions and outlook

NDs have received a considerable interest owing to their non-toxicity, chemical inertness and hardness due to sp^3 bonding structure, easy surface functionalization due to sp^2 graphitic shell, optical properties suitable for use as FI probes, and paramagnetic and ferromagnetic properties suitable for use as MRI probes. NDs can be produced using various methods as reviewed here. In addition, they are commercially available at reasonable prices.

Although pure NDs are colorless and optically transparent, NDs with NVs as color centers are fluorescent in the red region, which are extremely useful as FI probes. In addition, conjugation of octadecylamine to NDs allowed blue photon emissions. Their potential as FI probes has been demonstrated *via in vitro* and *in vivo* experiments. Compared with organic dyes and quantum dots (QDs), color centers of NDs are extremely photostable with no photobleaching and quenching owing to their location at the ND center and protection by strong sp^3 structure. Very high quantum yields close to one supports the superiority of NDs as FI probes.

Pure NDs are diamagnetic owing to a closed-shell sp^3 electronic structure. However, NDs are paramagnetic owing to defect structures such as NVs and sp^2 surface graphitic carbons. NDs can be even ferromagnetic after thermal treatment or after ion irradiation with ^{15}N and ^{12}C. These paramagnetic and ferromagnetic properties of NDs make them useful as MRI probes. The paramagnetic properties had been successfully applied to MRI *in vitro* and *in vivo* whereas the ferromagnetic properties have not been applied to MRI so far. Considering that the ferromagnetic NDs can be applied as T_2 MRI probes such as iron oxide nanoparticles, studies of ferromagnetic NDs as T_2 MRI probes will be highly appreciated.

The fluorescent intensity of NDs is typically lower than those of organic dyes and quantum dots. Therefore, NDs with a high density of NV centers must be developed because their fluorescent intensity is proportional to the amount of NV centers per ND. On the other hand, for biomedical applications, small and size-controlled NDs ($d < 3$ nm) are preferred to ensure their renal excretion from the body, but small NDs have a small amount of NV centers, leading to reduced fluorescence intensity. Therefore, it will be extremely useful to develop size-controlled, small NDs ($d < 3$ nm) with a high density of NV centers. Although NDs do not cause biotoxicity in the body, they are not metabolized in the body. Therefore, synthesis of small and brightly fluorescent NDs on a large scale is a great future challenge.

Considering excellent optical and magnetic properties including outstanding biocompatibility,[163] NDs are considered as potential dual-modal FI and MRI probes. ND surfaces can be easily conjugated with hydrophilic ligands for colloidal stability in aqueous media for biomedical applications. Further, ND surfaces can be conjugated with various functional molecules, antibodies, and drugs for further advanced applications. Therefore, NDs can serve as a new class of promising probes for theranostic biomedical applications in the future.

Abbreviations

A549	Human lung epithelial cell
bSSFP	Balanced steady-state free precession
C	Caenorhabditis
CB	Carbon black
CdO	Cadmium oxide
CVD	Chemical vapor deposition
DLS	Dynamic light scattering
DND3	De-agglutinated detonation nanodiamond colloid
EDC	1-Ethyl-3-(3-dimethylaminopropyl)carbodiimide
EDS	Energy dispersive X-ray spectroscopy
EPR	Electron paramagnetic resonance
HEK293	Human embryonic kidney 293 cell
HPHT	High pressure and high temperature
TEM	Transmission electron microscope
FI	Fluorescence imaging
LND	Laser-synthesized ND
MRI	Magnetic resonance imaging

© 2023 The Author(s). Published by the Royal Society of Chemistry

Open Access Article. Published on 03 November 2023. Downloaded on 2/10/2026 5:30:09 AM. This article is licensed under a Creative Commons Attribution-NonCommercial 3.0 Unported Licence.

MTT	3-(4,5-Dimethylthiazol-2-yl)-2,5-diphenyltetrazolium bromide
ND	Nanodiamond
NHS	*N*-Hydroxysuccinimide
NMR	Nuclear magnetic resonance
NV	Nitrogen vacancy
OMRI	Overhauser-enhanced MRI
PBS	Phosphate buffer solution
PEG	Plyethylene glycol
PEI	Polyethylenimine
QD	Quantum dot
SIP	Selective imaging protocol
HEK293T	Human embryonic kidney 293 tumor cell
XRD	X-ray diffraction

Conflicts of interest

There are no conflicts to declare.

Acknowledgements

This work was supported by the Basic Science Research Program of the National Research Foundation (NRF) funded by the Korea government (Ministry of Science, and Information and Communications Technology: MSIT) (Basic Research Laboratory, No. 2021R1A4A1029433).

Notes and references

1 A. S. Thakor, J. V. Jokerst, P. Ghanouni, J. L. Campbell, E. Mittra and S. S. Gambhir, *J. Nucl. Med.*, 2016, **57**, 1833–1837.
2 J. Kim, N. Lee and T. Hyeon, *Philos. Trans. R. Soc., A*, 2017, **375**, 20170022.
3 E. B. Ehlerding, P. Grodzinski, W. Cai and C. H. Liu, *ACS Nano*, 2018, **12**, 2106–2121.
4 R. M. Crist, S. S. K. Dasa, C. H. Liu, J. D. Clogston, M. A. Dobrovolskaia and S. T. Stern, *Wiley Interdiscip. Rev.: Nanomed. Nanobiotechnol.*, 2021, **13**, e1665.
5 H. Dong, S.-R. Du, X.-Y. Zheng, G.-M. Lyu, L.-D. Sun, L.-D. Li, P.-Z. Zhang, C. Zhang and C.-H. Yan, *Chem. Rev.*, 2015, **115**, 10725–10815.
6 D. Kim, J. Kim, Y. I. Park, N. Lee and T. Hyeon, *ACS Cent. Sci.*, 2018, **4**, 324–336.
7 S. Sabella, R. P. Carney, V. Brunetti, M. A. Malvindi, N. A. Juffali, G. Vecchio, S. M. Janes, O. M. Bakr, R. Cingolani, F. Stellacci and P. P. Pompa, *Nanoscale*, 2014, **6**, 7052–7061.
8 L. S. Arias, J. P. Pessan, A. P. M. Vieira, T. M. T. de Lima, A. C. B. Delbem and D. R. Monteiro, *Antibiotics*, 2018, **7**, 46.
9 Y. H. Hu, *Small*, 2014, **10**, 1451–1452.
10 T. Tegafaw, I. T. Oh, H. Cha, H. Yue, X. Miao, S. L. Ho, M. Y. Ahmad, S. Marasini, A. Ghazanfari, H. K. Kim, K. S. Chae, Y. Chang and G. H. Lee, *J. Phys. Chem. Solids*, 2018, **120**, 96–103.
11 G. Hong, S. Diao, A. L. Antaris and H. Dai, *Chem. Rev.*, 2015, **115**, 10816–10906.
12 O. A. Shenderova and G. E. McGuire, *Biointerphases*, 2015, **10**, 030802.
13 A. Shakun, J. Vuorinen, M. Hoikkanen, M. Poikelispää and A. Das, *Composites, Part A*, 2014, **64**, 49–69.
14 M. B. A. Olia, P. S. Donnelly, L. C. L. Hollenberg, P. Mulvaney and D. A. Simpson, *ACS Appl. Nano Mater.*, 2021, **4**, 9985–10005.
15 A. Wolcott, T. Schiros, M. E. Trusheim, E. H. Chen, D. Nordlund, R. E. Diaz, O. Gaathon, D. Englund and J. S. Owen, *J. Phys. Chem. C*, 2014, **118**, 26695–26702.
16 A. Freedman, *J. Appl. Phys.*, 1994, **75**, 3112–3120.
17 J.-C. Arnault, T. Petit, H. Girard, A. Chavanne, C. Gesset, M. Sennour and M. Chaigneau, *Phys. Chem. Chem. Phys.*, 2011, **13**, 11481–11487.
18 K.-I. Sotowa, T. Amamoto, A. Sobana, K. Kusakabe and T. Imato, *Diamond Relat. Mater.*, 2004, **13**, 145–150.
19 W.-W. Zheng, Y.-H. Hsieh, Y.-C. Chiu, S.-J. Cai, C.-L. Cheng and C. Chen, *J. Mater. Chem.*, 2009, **19**, 8432–8441.
20 T. Petit, J.-C. Arnault, H. A. Girard, M. Sennour and P. Bergonzo, *Phys. Rev. B: Condens. Matter Mater. Phys.*, 2011, **84**, 233407.
21 M. Lu, Y. K. Wang, J. Zhao, H. Lu, M. H. Stenzel and P. Xiao, *Macromol. Rapid Commun.*, 2016, **37**, 2023–2029.
22 S. Vial, C. Mansuy, S. Sagan, T. Irinopoulou, F. Burlina, J.-P. Boudou, G. Chassaing and S. Lavielle, *ChemBioChem*, 2008, **9**, 2113–2119.
23 B.-M. Chang, H.-H. Lin, L.-J. Su, W.-D. Lin, R.-J. Lin, Y.-K. Tzeng, R. T. Lee, Y. C. Lee, A. L. Yu and H.-C. Chang, *Adv. Funct. Mater.*, 2013, **23**, 5737–5745.
24 C. Gaillard, H. A. Girard, C. Falck, V. Paget, V. Simic, N. Ugolin, P. Bergonzo, S. Chevillard and J. C. Arnault, *RSC Adv.*, 2014, **4**, 3566–3572.
25 K.-K. Liu, W.-W. Zheng, C.-C. Wang, Y.-C. Chiu, C.-L. Cheng, Y.-S. Lo, C. Chen and J.-I. Chao, *Nanotechnology*, 2010, **21**, 315106.
26 H.-D. Wang, Q. Yang, C. Hui Niu and I. Badea, *Diamond Relat. Mater.*, 2012, **26**, 1–6.
27 J. Neburkova, F. Sedlak, J. Z. Suchanova, L. Kostka, P. Sacha, V. Subr, T. Etrych, P. Simon, J. Barinkova, R. Krystufek, H. Spanielova, J. Forstova, J. Konvalinka and P. Cigler, *Mol. Pharm.*, 2018, **15**, 2932–2945.
28 A. Barras, J. Lyskawa, S. Szunerits, P. Woisel and R. Boukherroub, *Langmuir*, 2011, **27**, 12451–12457.
29 J. Slegerova, M. Hajek, I. Rehor, F. Sedlak, J. Stursa, M. Hruby and P. Cigler, *Nanoscale*, 2015, **7**, 415–420.
30 C. Presti, J. G. Alauzun, D. Laurencin and P. H. Mutin, *Langmuir*, 2014, **30**, 9239–9245.
31 A. Krüger, Y. Liang, G. Jarre and J. Stegk, *J. Mater. Chem.*, 2006, **16**, 2322–2328.
32 Y. Wu, A. Ermakova, W. Liu, G. Pramanik, T. M. Vu, A. Kurz, L. McGuinness, B. Naydenov, S. Hafner, R. Reuter, J. Wrachtrup, J. Isoya, C. Förtsch, H. Barth, T. Simmet, F. Jelezko and T. Weil, *Adv. Funct. Mater.*, 2015, **25**, 6576–6585.

© 2023 The Author(s). Published by the Royal Society of Chemistry

Open Access Article. Published on 03 November 2023. Downloaded on 2/10/2026 5:30:09 AM. This article is licensed under a Creative Commons Attribution-NonCommercial 3.0 Unported Licence.

33 R. Kaur, J. M. Chitanda, D. Michel, J. Maley, F. Borondics, P. Yang, R. E. Verrall and I. Badea, *Int. J. Nanomed.*, 2012, **7**, 3851–3866.
34 C. C. Fu, H. Y. Lee, K. Chen, T. S. Lim, H. Y. Wu, P. K. Lin, P. K. Wei, P. H. Tsao, H. C. Chang and W. Fann, *Proc. Natl. Acad. Sci. U. S. A.*, 2007, **104**, 727–732.
35 S. Claveau, J.-R. Bertrand and F. Treussart, *Micromachines*, 2018, **9**, 247.
36 A. M. Panich, M. Salti, S. D. Goren, E. B. Yudina, A. E. Aleksenskii, A. Y. Vul' and A. I. Shames, *J. Phys. Chem. C*, 2019, **123**, 2627–2631.
37 L. M. Manus, D. J. Mastarone, E. A. Waters, X.-Q. Zhang, E. A. S. Sikma, K. W. MacRenaris, D. Ho and T. J. Meade, *Nano Lett.*, 2010, **10**, 484–489.
38 N. Rammohan, K. W. MacRenaris, L. K. Moore, G. Parigi, D. J. Mastarone, L. M. Manus, L. M. Lilley, A. T. Preslar, E. A. Waters, A. Filicko, C. Luchinat, D. Ho and T. J. Meade, *Nano Lett.*, 2016, **16**, 7551–7564.
39 L. Zhao, A. Shiino, H. Qin, T. Kimura and N. Komatsu, *J. Nanosci. Nanotechnol.*, 2015, **15**, 1076–1082.
40 A. M. Panich, A. I. Shames, N. A. Sergeev, V. Y. Osipov, A. E. Alexenskiy and A. Y. Vul', *J. Phys. Chem. C*, 2016, **120**, 19804–19811.
41 A. M. Panich, A. I. Shames, O. Medvedev, V. Y. Osipov, A. E. Aleksenskiy and A. Y. Vul', *Appl. Magn. Reson.*, 2009, **36**, 317–329.
42 W. Hou, T. B. Toh, L. N. Abdullah, T. W. Z. Yvonne, K. J. Lee, I. Guenther and E. K.-H. Chow, *Nanomed.: Nanotechnol. Biol. Med.*, 2017, **13**, 783–793.
43 A. I. Shames, A. M. Panich, V. Y. Osipov, A. E. Aleksenskiy, A. Y. Vul', T. Enoki and K. Takai, *J. Appl. Phys.*, 2010, **107**, 014318.
44 A. M. Panich, A. Altman, A. I. Shames, V. Y. Osipov, A. E. Aleksenskiy and A. Y. Vul', *J. Phys. D: Appl. Phys.*, 2011, **44**, 125303.
45 D. E. J. Waddington, M. Sarracanie, H. Zhang, N. Salameh, D. R. Glenn, E. Rej, T. Gaebel, T. Boele, R. L. Walsworth, D. J. Reilly and M. S. Rosen, *Nat. Commun.*, 2017, **8**, 15118.
46 N. Prabhakar and J. M. Rosenholm, *Curr. Opin. Colloid Interface Sci.*, 2019, **39**, 220–231.
47 K. V. Volkov, V. V. Danilenko and V. I. Elin, *Combust. Explos. Shock Waves*, 1990, **26**, 366–368.
48 V. Y. Dolmatov, A. N. Ozerin, I. I. Kulakova, O. O. Bochechka, N. M. Lapchuk, V. Myllymäki and A. Vehanen, *Russ. Chem. Rev.*, 2020, **89**, 1428–1462.
49 I. M. Abdullahi, M. Langenderfer, O. Shenderova, N. Nunn, M. D. Torelli, C. E. Johnson and V. N. Mochalin, *Carbon*, 2020, **164**, 442–450.
50 J.-P. Boudou, J. Tisler, R. Reuter, A. Thorel, P. A. Curmi, F. Jelezko and J. Wrachtrup, *Diamond Relat. Mater.*, 2013, **37**, 80–86.
51 D. Amans, A.-C. Chenus, G. Ledoux, C. Dujardin, C. Reynaud, O. Sublemontier, K. M. Varlot and O. Guillois, *Diamond Relat. Mater.*, 2009, **18**, 177–180.
52 S. Hu, J. Sun, X. Du, F. Tian and L. Jiang, *Diamond Relat. Mater.*, 2008, **17**, 142–146.
53 L. Basso, F. Gorrini, N. Bazzanella, M. Cazzanelli, C. Dorigoni, A. Bifone and A. Miotello, *Appl. Phys. A*, 2018, **124**, 72.
54 H.-Y. Kim, D.-S. Kim and N.-M. Hwang, *RSC Adv.*, 2021, **11**, 5651–5657.
55 E. Tamburri, R. Carcione, F. Vitale, A. Valguarnera, S. Macis, M. Lucci and M. L. Terranova, *Adv. Mater. Interfaces*, 2017, **4**, 1700222.
56 P. W. May, M. N. R. Ashfold and Y. A. Mankelevich, *J. Appl. Phys.*, 2007, **101**, 053115.
57 S. Welz, Y. Gogotsi and M. J. McNallan, *J. Appl. Phys.*, 2003, **93**, 4207–4214.
58 A. K. Khachatryan, S. G. Aloyan, P. W. May, R. Sargsyan, V. A. Khachatryan and V. S. Baghdasaryan, *Diamond Relat. Mater.*, 2008, **17**, 931–936.
59 T. L. Daulton, M. A. Kirk, R. S. Lewis and L. E. Rehn, *Nucl. Instrum. Methods Phys. Res. Sect. B*, 2001, **175–177**, 12–20.
60 F. Banhart and P. M. Ajayan, *Nature*, 1996, **382**, 433–435.
61 I. Rehor and P. Cigler, *Diamond Relat. Mater.*, 2014, **46**, 21–24.
62 A. P. Puzyr, A. E. Burova, V. S. Bondar, C. K. Rhee, W. H. Rhee and K. C. Hwang, *J. Korean Powder Metall. Inst.*, 2011, **18**, 297–302.
63 A. Brož, L. Bačáková, P. Štenclová, A. Kromka and Š. Potocký, *Beilstein J. Nanotechnol.*, 2017, **8**, 1649–1657.
64 V. N. Mochalin, O. Shenderova, D. Ho and Y. Gogotsi, *Nat. Nanotechnol.*, 2012, **7**, 11–23.
65 V. Pichot, B. Risse, F. Schnell, J. Mory and D. Spitzer, *Sci. Rep.*, 2013, **3**, 2159.
66 V. Y. Dolmatov, *Russ. Chem. Rev.*, 2001, **70**, 607–626.
67 S. P. Hong, S. W. Ha and S. W. Lee, *Diamond Relat. Mater.*, 2018, **81**, 27–32.
68 S. Ha, S. P. Hong, M. Lee, S. Lee and S. W. Lee, *Mater. Today Commun.*, 2019, **21**, 100571.
69 O. Shenderova, A. Koscheev, N. Zaripov, I. Petrov, Y. Skryabin, P. Detkov, S. Turner and G. Van Tendeloo, *J. Phys. Chem. C*, 2011, **115**, 9827–9837.
70 J. Ackermann and A. Krueger, *Nanoscale*, 2019, **11**, 8012–8019.
71 S. Osswald, G. Yushin, V. Mochalin, S. O. Kucheyev and Y. Gogotsi, *J. Am. Chem. Soc.*, 2006, **128**, 11635–11642.
72 C. Bradac and S. Osswald, *Carbon*, 2018, **132**, 616–622.
73 A. Krüger, F. Kataoka, M. Ozawa, T. Fujino, Y. Suzuki, A. E. Aleksenskii, A. Y. Vul' and E. Ōsawa, *Carbon*, 2005, **43**, 1722–1730.
74 S. Stehlik, J. Henych, P. Stenclova, R. Kral, P. Zemenova, J. Pangrac, O. Vanek, A. Kromka and B. Rezek, *Carbon*, 2021, **171**, 230–239.
75 S. Gupta, B. Evans, A. Henson and S. B. Carrizosa, *Materials*, 2017, **10**, 1292.
76 A. Pentecost, S. Gour, V. Mochalin, I. Knoke and Y. Gogotsi, *ACS Appl. Mater. Interfaces*, 2010, **2**, 3289–3294.
77 S. Stehlik, M. Varga, M. Ledinsky, V. Jirasek, A. Artemenko, H. Kozak, L. Ondic, V. Skakalova, G. Argentero, T. Pennycook, J. C. Meyer, A. Fejfar, A. Kromka and B. Rezek, *J. Phys. Chem. C*, 2015, **119**, 27708–27720.

© 2023 The Author(s). Published by the Royal Society of Chemistry

Open Access Article. Published on 03 November 2023. Downloaded on 2/10/2026 5:30:09 AM. This article is licensed under a Creative Commons Attribution-NonCommercial 3.0 Unported Licence.

78 M. Kasu, *Prog. Cryst. Growth Charact. Mater.*, 2016, **62**, 317–328.
79 R. Kumar, S. J. Yoon, K. G. Lee, P. Pal, R. P. Pant, C. K. Suman, S. R. Dhakate, R. Kumar, D. K. Avasthi and D. K. Singh, *RSC Adv.*, 2016, **6**, 47164–47173.
80 F. Gorrini, M. Cazzanelli, N. Bazzanella, R. Edla, M. Gemmi, V. Cappello, J. David, C. Dorigoni, A. Bifone and A. Miotello, *Sci. Rep.*, 2016, **6**, 35244.
81 L. Yang, P. W. May, L. Yin, J. A. Smith and K. N. Rosser, *Diamond Relat. Mater.*, 2007, **16**, 725–729.
82 J.-W. Park, K.-S. Kim and N.-M. Hwang, *Carbon*, 2016, **106**, 289–294.
83 J. E. Butler and A. V. Sumant, *Chem. Vap. Deposition*, 2008, **14**, 145–160.
84 P. Stenclova, V. Celedova, A. Artemenko, V. Jirasek, J. Jira, B. Rezek and A. Kromka, *RSC Adv.*, 2017, **7**, 38973–38980.
85 A. T. Kozakov, A. G. Kochur, N. Kumar, K. Panda, A. V. Nikolskii and A. V. Sidashov, *Appl. Surf. Sci.*, 2021, **536**, 147807.
86 J. Xiao, P. Liu and G. W. Yang, *Nanoscale*, 2015, **7**, 6114–6125.
87 H.-S. Jung and K. C. Neuman, *Nanomaterials*, 2021, **11**, 153.
88 T. Ando, J. Tanaka, M. Ishii, M. Kamo, Y. Sato, N. Ohashi and S. Shimosaki, *J. Chem. Soc. Faraday Trans.*, 1993, **89**, 3105–3109.
89 M. Börsch, R. Reuter, G. Balasubramanian, R. Erdmann, F. Jelezko and J. Wrachtrup, *Proc. SPIE*, 2009, **7183**, 71832N.
90 A. Bumb, S. K. Sarkar, N. Billington, M. W. Brechbiel and K. C. Neuman, *J. Am. Chem. Soc.*, 2013, **135**, 7815–7818.
91 N. Prabhakar, T. Näreoja, E. von Haartman, D. Ş. Karaman, H. Jiang, S. Koho, T. A. Dolenko, P. E. Hänninen, D. I. Vlasov, V. G. Ralchenko, S. Hosomi, I. I. Vlasov, C. Sahlgren and J. M. Rosenholm, *Nanoscale*, 2013, **5**, 3713–3722.
92 D. Wang, Y. Tong, Y. Li, Z. Tian, R. Cao and B. Yang, *Diamond Relat. Mater.*, 2013, **36**, 26–34.
93 A. S. Barnard, *Nanoscale*, 2017, **9**, 70–74.
94 X. Zhang, C. Fu, L. Feng, Y. Ji, L. Tao, Q. Huang, S. Li and Y. Wei, *Polymer*, 2012, **53**, 3178–3184.
95 G. Yang, W. Long, W. Yan, H. Huang, M. Liu, H. Ouyang, Y. Feng, L. Liu, X. Zhang and Y. Wei, *J. Drug Delivery Sci. Technol.*, 2020, **57**, 101644.
96 L. Zhao, Y.-H. Xu, T. Akasaka, S. Abe, N. Komatsu, F. Watari and X. Chen, *Biomaterials*, 2014, **35**, 5393–5406.
97 J.-P. Boudou, M.-O. David, V. Joshi, H. Eidi and P. A. Curmi, *Diamond Relat. Mater.*, 2013, **38**, 131–138.
98 L. Zhao, T. Takimoto, M. Ito, N. Kitagawa, T. Kimura and N. Komatsu, *Angew. Chem., Int. Ed.*, 2011, **50**, 1388–1392.
99 M. Chen, X.-Q. Zhang, H. B. Man, R. Lam, E. K. Chow and D. Ho, *J. Phys. Chem. Lett.*, 2010, **1**, 3167–3171.
100 S. Qin, M. Cui, S. Qiu, H. Zhao, L. Wang and A. Zhang, *RSC Adv.*, 2018, **8**, 3694–3704.
101 S. P. Santana, N. F. Salazar, A. S. Sainz, E. S. Campa, A. B. Estrella, A. A. Molina, R. Melendrez, M. P. Montero and R. Riera, *Adv. Nat. Sci.: Nanosci. Nanotechnol.*, 2018, **9**, 015013.
102 Y. Dong, R. Cao, Y. Li, Z. Wang, L. Li and L. Tian, *RSC Adv.*, 2015, **5**, 82711–82716.
103 L. Li, L. Tian, W. Zhao, F. Cheng, Y. Li and B. Yang, *RSC Adv.*, 2016, **6**, 36407–36417.
104 V. N. Mochalin and Y. Gogotsi, *J. Am. Chem. Soc.*, 2009, **131**, 4594–4595.
105 P. Karami and A. Shojaei, *Polym. Int.*, 2017, **66**, 557–565.
106 D. G. Lim, K. H. Kim, E. Kang, S. H. Lim, J. Ricci, S. K. Sung, M. T. Kwon and S. H. Jeong, *Int. J. Nanomed.*, 2016, **11**, 2381–2395.
107 D. Wang, Y. Li, Z. Tian, R. Cao and B. Yang, *Ther. Delivery*, 2014, **5**, 511–524.
108 D. Meziane, A. Barras, A. Kromka, J. Houdkova, R. Boukherroub and S. Szunerits, *Anal. Chem.*, 2012, **84**, 194–200.
109 L. Marcon, Z. Kherrouche, J. Lyskawa, D. Fournier, D. Tulasne, P. Woisel and R. Boukherroub, *Chem. Commun.*, 2011, **47**, 5178–5180.
110 A. Barras, S. Szunerits, L. Marcon, N. M. Dupont and R. Boukherroub, *Langmuir*, 2010, **26**, 13168–13172.
111 A. Krueger and T. Boedeker, *Diamond Relat. Mater.*, 2008, **17**, 1367–1370.
112 J.-P. Boudou, P. A. Curmi, F. Jelezko, J. Wrachtrup, P. Aubert, M. Sennour, G. Balasubramanian, R. Reuter, A. Thorel and E. Gaffet, *Nanotechnology*, 2009, **20**, 235602.
113 V. Kuzmin, K. Safiullin, G. Dolgorukov, A. Stanislavovas, E. Alakshin, T. Safin, B. Yavkin, S. Orlinskii, A. Kiiamov, M. Presnyakov, A. Klochkov and M. Tagirov, *Phys. Chem. Chem. Phys.*, 2018, **20**, 1476–1484.
114 M. V. Baidakova, Y. A. Kukushkina, A. A. Sitnikova, M. A. Yagovkina, D. A. Kirilenko, V. V. Sokolov, M. S. Shestakov, A. Y. Vul', B. Zousman and O. Levinson, *Phys. Solid State*, 2013, **55**, 1747–1753.
115 V. I. Korepanov, H.-o. Hamaguchi, E. Osawa, V. Ermolenkov, I. K. Lednev, B. J. M. Etzold, O. Levinson, B. Zousman, C. P. Epperla and H.-C. Chang, *Carbon*, 2017, **121**, 322–329.
116 S. S. Batsanov, S. M. Gavrilkin, A. S. Batsanov, K. B. Poyarkov, I. I. Kulakova, D. W. Johnson and B. G. Mendis, *J. Mater. Chem.*, 2012, **22**, 11166–11172.
117 J. Xiao, P. Liu, L. Li and G. Yang, *J. Phys. Chem. C*, 2015, **119**, 2239–2248.
118 K. N. Clayton, J. W. Salameh, S. T. Wereley and T. L. Kinzer-Ursem, *Biomicrofluidics*, 2016, **10**, 054107.
119 C. Fryer, P. Murray and H. Zhang, *Nanomaterials*, 2022, **12**, 4196.
120 C. D. C. Wachesk, C. R. Hurtado, R. F. B. D. O. Correia, D. B. Tada, G. Vasconcelos, E. J. Corat and V. J. T. Airoldi, *Biomed. J. Sci. Tech. Res.*, 2022, **41**, 32695–32709.
121 D. Maziukiewicz, R. Mrówczyński, S. Jurga and B. F. Grześkowiak, *Diamond Relat. Mater.*, 2022, **128**, 109308.
122 E. R. Wilson, L. M. Parker, A. Orth, N. Nunn, M. Torelli, O. Shenderova, B. C. Gibson and P. Reineck, *Nanotechnology*, 2019, **30**, 385704.

Open Access Article. Published on 03 November 2023. Downloaded on 2/10/2026 5:30:09 AM. This article is licensed under a Creative Commons Attribution-NonCommercial 3.0 Unported Licence.

123 W. Cao, X. Peng, X. Chen, X. Wang, F. Jin, Q. Li, H. Chen, C. Jiang, Z. Ye and X. Xing, *J. Mater. Sci.*, 2017, **52**, 1856–1867.
124 X. Xu, Z. Yu, Y. Zhu and B. Wang, *Diamond Relat. Mater.*, 2005, **14**, 206–212.
125 L. Zhao, Y. Nakae, H. Qin, T. Ito, T. Kimura, H. Kojima, L. Chan and N. Komatsu, *Beilstein J. Org. Chem.*, 2014, **10**, 707–713.
126 L. Gines, S. Mandal, A. I. Ahmad, C.-L. Cheng, M. Sow and O. A. Williams, *Nanoscale*, 2017, **9**, 12549–12555.
127 Y.-R. Chang, H.-Y. Lee, K. Chen, C.-C. Chang, D.-S. Tsai, C.-C. Fu, T.-S. Lim, Y.-K. Tzeng, C.-Y. Fang, C.-C. Han, H.-C. Chang and W. Fann, *Nat. Nanotechnol.*, 2008, **3**, 284–288.
128 J. Havlik, V. Petrakova, I. Rehor, V. Petrak, M. Gulka, J. Stursa, J. Kucka, J. Ralis, T. Rendler, S.-Y. Lee, R. Reuter, J. Wrachtrup, M. Ledvina, M. Nesladek and P. Cigler, *Nanoscale*, 2013, **5**, 3208–3211.
129 G. Dantelle, A. Slablab, L. Rondin, F. Lainé, F. Carrel, P. Bergonzo, S. Perruchas, T. Gacoin, F. Treussart and J. F. Roch, *J. Lumin.*, 2010, **130**, 1655–1658.
130 Y. Y. Hui, Y.-R. Chang, N. Mohan, T.-S. Lim, Y.-Y. Chen and H.-C. Chang, *J. Phys. Chem. A*, 2011, **115**, 1878–1884.
131 S.-J. Yu, M.-W. Kang, H.-C. Chang, K.-M. Chen and Y.-C. Yu, *J. Am. Chem. Soc.*, 2005, **127**, 17604–17605.
132 L. Rondin, G. Dantelle, A. Slablab, F. Grosshans, F. Treussart, P. Bergonzo, S. Perruchas, T. Gacoin, M. Chaigneau, H.-C. Chang, V. Jacques and J.-F. Roch, *Phys. Rev. B: Condens. Matter Mater. Phys.*, 2010, **82**, 115449.
133 H.-C. Lu, Y.-C. Peng, S.-L. Chou, J.-I. Lo, B.-M. Cheng and H.-C. Chang, *Angew. Chem., Int. Ed.*, 2017, **56**, 14469–14473.
134 E. von Haartman, H. Jiang, A. A. Khomich, J. Zhang, S. A. Burikov, T. A. Dolenko, J. Ruokolainen, H. Gu, O. A. Shenderova, I. I. Vlasov and J. M. Rosenholm, *J. Mater. Chem. B*, 2013, **1**, 2358–2366.
135 S. Sotoma, F.-J. Hsieh, Y.-W. Chen, P.-C. Tsai and H.-C. Chang, *Chem. Commun.*, 2018, **54**, 1000–1003.
136 P. G. Baranov, A. A. Soltamova, D. O. Tolmachev, N. G. Romanov, R. A. Babunts, F. M. Shakhov, S. V. Kidalov, A. Y. Vul', G. V. Mamin, S. B. Orlinskii and N. I. Silkin, *Small*, 2011, **7**, 1533–1537.
137 W. Liu, M. N. A. Alam, Y. Liu, V. N. Agafonov, H. Qi, K. Koynov, V. A. Davydov, R. Uzbekov, U. Kaiser, T. Lasser, F. Jelezko, A. Ermakova and T. Weil, *Nano Lett.*, 2022, **22**, 2881–2888.
138 Y. Makino, T. Mahiko, M. Liu, A. Tsurui, T. Yoshikawa, S. Nagamachi, S. Tanaka, K. Hokamoto, M. Ashida, M. Fujiwara, N. Mizuochi and M. Nishikawa, *Diamond Relat. Mater.*, 2021, **112**, 108248.
139 E. Perevedentseva, A. Karmenyan, Y. C. Lin, C. Y. Song, Z. R. Lin, A. I. Ahmed, C. C. Chang, S. Norina, V. Bessalova, N. Perov, O. Levinson, B. Zousman and C.-L. Cheng, *J. Biomed. Opt.*, 2018, **23**, 091404.
140 V. Y. Osipov, A. I. Shames, T. Enoki, K. Takai, M. V. Baidakova and A. Y. Vul', *Diamond Relat. Mater.*, 2007, **16**, 2035–2038.
141 A. I. Shames, A. M. Panich, W. Kempiński, A. E. Alexenskii, M. V. Baidakova, A. T. Dideikin, V. Y. Osipov, V. I. Siklitski, E. Osawa, M. Ozawa and A. Y. Vul, *J. Phys. Chem. Solids*, 2002, **63**, 1993–2001.
142 I. Kratochvílova, J. Šebera, P. Ashcheulov, M. Golan, M. Ledvina, J. Míčova, F. Mravec, A. Kovalenko, D. Zverev, B. Yavkin, S. Orlinskii, S. Záliš, A. Fišerová, J. Richter, L. Šefc and J. Turánek, *J. Phys. Chem. C*, 2014, **118**, 25245–25252.
143 Z. Peng, J. Dallas and S. Takahashi, *J. Appl. Phys.*, 2020, **128**, 054301.
144 S. Talapatra, P. G. Ganesan, T. Kim, R. Vajtai, M. Huang, M. Shima, G. Ramanath, D. Srivastava, S. C. Deevi and P. M. Ajayan, *Phys. Rev. Lett.*, 2005, **95**, 097201.
145 A. Setzer, P. D. Esquinaz, S. Buga, M. T. Georgieva, T. Reinert, T. Venus, I. Eestrela-Lopis, A. Ivashenko, M. Bondarenko, W. Böhlmann and J. Meijer, *Materials*, 2022, **15**, 1014.
146 A. M. Schrand, L. Dai, J. J. Schlager, S. M. Hussain and E. Osawa, *Diamond Relat. Mater.*, 2007, **16**, 2118–2123.
147 C. Cheng, A. E. Porter, K. Muller, K. Koziol, J. N. Skepper, P. Midgley and M. Welland, *J. Phys. Conf. Ser.*, 2009, **151**, 012030.
148 Y. Zhu, J. Li, W. Li, Y. Zhang, X. Yang, N. Chen, Y. Sun, Y. Zhao, C. Fan and Q. Huang, *Theranostics*, 2012, **2**, 302–312.
149 V. Paget, J. A. Sergent, R. Grall, S. A. Morel, H. A. Girard, T. Petit, C. Gesset, M. Mermoux, P. Bergonzo, J. C. Arnault and S. Chevillard, *Nanotoxicology*, 2014, **8**, 46–56.
150 A. M. Schrand, H. Huang, C. Carlson, J. J. Schlager, E. Ōsawa, S. M. Hussain and L. Dai, *J. Phys. Chem. B*, 2007, **111**, 2–7.
151 X. Zhang, W. Hu, J. Li, L. Tao and Y. Wei, *Toxicol. Res.*, 2012, **1**, 62–68.
152 X. Zhang, J. Yin, C. Kang, J. Li, Y. Zhu, W. Li, Q. Huang and Z. Zhu, *Toxicol. Lett.*, 2010, **198**, 237–243.
153 L. Marcon, F. Riquet, D. Vicogne, S. Szunerits, J.-F. Bodart and R. Boukherroub, *J. Mater. Chem.*, 2010, **20**, 8064–8069.
154 N. Dworak, M. Wnuk, J. Zebrowski, G. Bartosz and A. Lewinska, *Carbon*, 2014, **68**, 763–776.
155 K. Solarska, A. Gajewska, W. Kaczorowski, G. Bartosz and K. Mitura, *Diamond Relat. Mater.*, 2012, **21**, 107–113.
156 A. P. Puzyr, D. A. Neshumayev, S. V. Tarskikh, G. V. Makarskaya, V. Y. Dolmatov and V. S. Bondar, *Diamond Relat. Mater.*, 2004, **13**, 2020–2023.
157 K. Turcheniuk and V. N. Mochalin, *Nanotechnology*, 2017, **28**, 252001.
158 M. Longmire, P. L. Choyke and H. Kobayashi, *Nanomedicine*, 2008, **3**, 703–717.
159 H. S. Choi, W. Liu, P. Misra, E. Tanaka, J. P. Zimmer, B. I. Ipe, M. G. Bawendi and J. V. Frangioni, *Nat. Biotechnol.*, 2007, **25**, 1165–1170.
160 S. Rojas, J. D. Gispert, R. Martin, S. Abad, C. Menchon, D. Pareto, V. M. Victor, M. Alvaro, H. Garcia and J. R. Herance, *ACS Nano*, 2011, **5**, 5552–5559.

© 2023 The Author(s). Published by the Royal Society of Chemistry

Open Access Article. Published on 03 November 2023. Downloaded on 2/10/2026 5:30:09 AM.
This article is licensed under a Creative Commons Attribution-NonCommercial 3.0 Unported Licence.

161 Y. Yuan, Y. Chen, J.-H. Liu, H. Wang and Y. Liu, *Diamond Relat. Mater.*, 2009, **18**, 95–100.
162 F. C. Barone, C. Marcinkiewicz, J. Li, Y. Feng, M. Sternberg, P. I. Lelkes, D. Rosenbaum-Halevi, J. A. Gerstenhaber and G. Z. Feuerstein, *Int. J. Nanomed.*, 2019, **14**, 1163–1175.
163 L. Moore, J. Yang, T. T. H. Lan, E. Osawa, D.-K. Lee, W. D. Johnson, J. Xi, E. K.-H. Chow and D. Ho, *ACS Nano*, 2016, **10**, 7385–7400.
164 J. C. Hsu, Z. Tang, O. E. Erenina, A. M. Soflas, T. Lammers, J. F. Lovell, C. Zavaleta, W. Cai and D. P. Cormode, *Nat. Rev. Method Primers*, 2023, **3**, 30.
165 L. M. Liz-Marzán, A. E. Nel, C. J. Brinker, W. C. W. Chan, C. Chen, X. Chen, D. Ho, T. Hu, K. Kataoka, N. A. Kotov, W. J. Parak and M. M. Stevens, *ACS Nano*, 2022, **16**, 13257–13259.
166 M. P. Lake and L.-S. Bouchard, *PLoS One*, 2017, **12**, e0179295.
167 H. M. Leung, M. S. Chan, L. S. Liu, S. W. Wong, T. W. Lo, C. H. Lau, C. Tin and P. K. Lo, *ACS Sustainable Chem. Eng.*, 2018, **6**, 9671–9681.
168 L. Nie, Y. Zhang, L. Li, P. van Rijn and R. Schirhagl, *Nanomaterials*, 2021, **11**, 1837.
169 P. Reineck, M. Capelli, D. W. M. Lau, J. Jeske, M. R. Field, T. Ohshima, A. D. Greentree and B. C. Gibson, *Nanoscale*, 2017, **9**, 497–502.
170 J.-I. Chao, E. Perevedentseva, P.-H. Chung, K.-K. Liu, C.-Y. Cheng, C.-C. Chang and C.-L. Cheng, *Biophys. J.*, 2007, **93**, 2199–2208.
171 R. Igarashi, Y. Yoshinari, H. Yokota, T. Sugi, F. Sugihara, K. Ikeda, H. Sumiya, S. Tsuji, I. Mori, H. Tochio, Y. Harada and M. Shirakawa, *Nano Lett.*, 2012, **12**, 5726–5732.
172 N. Mohan, C.-S. Chen, H.-H. Hsieh, Y.-C. Wu and H.-C. Chang, *Nano Lett.*, 2010, **10**, 3692–3699.
173 H. H. Han, H. Kang, S. Kim, R. Pal, A. T. N. Kumar, H. S. Choi and S. K. Hahn, *RSC Adv.*, 2021, **11**, 23073–23081.
174 M. D. Pham, C. P. Epperla, C.-L. Hsieh, W. Chang and H.-C. Chang, *Anal. Chem.*, 2017, **89**, 6527–6534.
175 D. E. J. Waddington, T. Boele, E. Rej, D. R. McCamey, N. J. C. King, T. Gaebel and D. J. Reilly, *Sci. Rep.*, 2019, **9**, 5950.
176 X. Lv, J. H. Walton, E. Druga, F. Wang, A. Aguilar, T. McKnelly, R. Nazaryan, F. L. Liu, L. Wu, O. Shenderova, D. B. Vigneron, C. A. Meriles, J. A. Reimer, A. Pines and A. Ajoy, *Proc. Natl. Acad. Sci. U. S. A.*, 2021, **118**, e2023579118.

© 2023 The Author(s). Published by the Royal Society of Chemistry